Increasing the Reliability of Lightning Protection of Electric Power Facilities

Marina Rezinkina, Vitalii Babak, Oleg Gryb, Artur Zaporozhets, and Oleg Rezinkin

Abstract The lightning protection system can become a factor in super-powerful electric fields, which is very dangerous for technical means that are located in such field, as example, unmanned aerial vehicles. But it is difficult to predict the cases when lightning strikes the current-carrying parts of electrical equipment. Therefore, it is necessary to have calculations on the distribution of fields during a lightning strike. This chapter presents models of the electric field in the vicinity of long thin wire rods and a model of the distribution of electric fields in the presence of an ionized streamer zone near the lightning top. The processes of corona at the tops of grounded rods, which imitate protected objects and lightning rods, are analyzed. The physical modeling of electromagnetic processes during the development of the corona on rod electrodes with different vertices has been performed.

Keywords Electric field · Lightning · Corona discharge · Corona current

1 Introduction

During choosing lightning protection means, data on the level of electromagnetic field (EF) strength in the "lightning leader—lightning rod" systems are needed. Studies aimed at solving the problem of calculating the EF in the vicinity of long thin conductive objects such as wires or rods, the length of which is on order of magnitude or more greater than their diameter, located in an external EF, are described in [1–5].

Direct measurement of the electrical parameters of such objects as the lightning leader channel presents significant difficulties. Therefore, their mathematical modeling has become widespread. During modeling the EF in systems containing long thin rods, a number of problems arise due to the large difference between their diameter and length. More often, long discharge channels are presented in the form

M. Rezinkina · O. Gryb · O. Rezinkin
National Technical University "Kharkiv Polytechnic Institute", Kharkiv, Ukraine

V. Babak · A. Zaporozhets (✉)
Institute of General Energy of NAS of Ukraine, Kyiv, Ukraine
e-mail: a.o.zaporozhets@nas.gov.ua

O. Kyrylenko et al. (eds.), *Power Systems Research and Operation*, Studies in Systems, Decision and Control 220, https://doi.org/10.1007/978-3-031-17554-1_13

of a charged filament [6]. It is also possible to use as a model of such objects an electrically conductive ellipsoid on which a charge located, as well as an electrically conductive ellipsoid located in a uniform external EF [7]. The closest model to real objects is the "cylinder in an external EF" model. It should be assessed how the choice of the rod model affects the distribution of potentials and strengths of the EF. When solving practical problems of lightning protection, analytical methods are mainly used, however, the use of numerical methods of calculation [8–10] makes it possible to take into account the real shape of lightning and lightning rods, the nature of the distribution of charges on them, the presence of ionized zones near them, as well as the influence of the earth on the magnitude and nature of the intensity distribution.

2 EF Simulation in the Vicinity of Thin Conductive Rods of Great Length

To assess the electrical parameters of a thin conductive channel in solving practical problems of lightning protection, as a rule, it is replaced by a filament with a charge uniformly distributed along its length. Then the distribution of potentials in the vicinity of an infinitely thin charged filament of length $2a$ located parallel to the Oz axis with center coordinates x_0, y_0, z_0 can be found using the well-known analytical expression [11]. However, in real systems, along the length of the leading rod, as a rule, not a charge, but a potential is given. It is known that the conductivity of the leader channel of lightning is quite large: for example, in [12] it is noted that the level of EF intensity in the leader channel is close to $E_L = 10^4$ V/m. Thus, in some approximation, the leader lightning channel can be considered the main and, during describing its EF, the analytical solution for the potential of free charges on the leading ellipsoid can be used [13, 14]. The performed calculations showed that the values of the potentials and strengths of the EF in the vicinity of sufficiently long and thin conductive rods, obtained by representing them in the form of a thin charged filament or a conducting ellipsoid, practically coincide, except that in the 2nd case there is an increase in the charge density and tension of the EF at the tops of the rods.

During calculating the parameters of the lightning leader channel, it should be taken into account that a real EF in a thunderstorm environment corresponds to a system that is a lightning leader channel located in a close to uniform external EF with strength E_0 (Fig. 1a). In this case, the well-known analytical solution for the leading prolate ellipsoid in the external EF can be used.

We assume that the ellipsoid is in a homogeneous EF with intensity E_0, directed along its major semi-axis a, parallel to the Oz axis, and its minor semi-axes are equal to each other: $b = c$. By transforming the expression for the potential outside the ellipsoid [14] for the case when its center has coordinates x_0, y_0, z_0, and taking the corresponding integrals, we finally obtain:

$$\varphi(x, y, z) = E_0 \cdot [z \cdot (1 - a_1/a_2) + z_0 \cdot a_1/a_2], \tag{1}$$

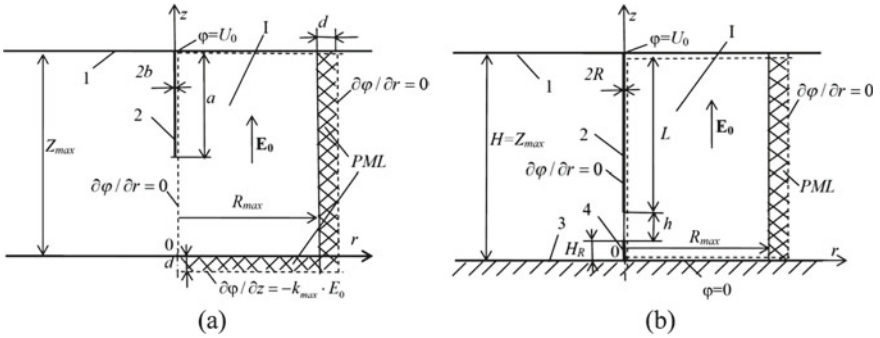

Fig. 1 Calculation system: **a** leader channel is located far from the ground in a EF with intensity E_0; **b** leader channel approaches to the ground and the lightning rod (1—upper limit of the considered area, 2—leader channel of the lightning, 3—ground, 4—lightning rod, – – – calculation area)

where $a_1 = -\frac{1}{(a^2-b^2)^{\frac{3}{2}}} \cdot \ln\frac{\sqrt{\xi+a^2}+\sqrt{a^2-b^2}}{\sqrt{\xi+a^2}-\sqrt{a^2-b^2}} + \frac{2}{(a^2-b^2)\cdot\sqrt{\xi+a^2}}$; $a_2 = -\frac{1}{(a^2-b^2)^{3/2}} \cdot \ln\frac{a+\sqrt{a^2-b^2}}{a-\sqrt{a^2-b^2}} + \frac{2}{(a^2-b^2)\cdot a}$; $\xi = -f_1 \pm \sqrt{f_1^2 - f_2}$; $f_1 = -\frac{(a^2+b^2)-[(x-x_0)^2+(y-y_0)^2+(z-z_0)^2]}{2}$; $f_2 = a^2b^2 - a^2 \cdot [(x-x_0)^2 + (y-y_0)^2] - b^2 \cdot (z-z_0)^2$.

2.1 *Statement of the Problem of Calculating the EF in the Vicinity of Conductive Rods of Great Length*

In some cases, to calculate the EF in the vicinity of conductive rods, it is necessary to use numerous methods. In [15] the numerical calculation of the EF distribution in such systems is described. Let us consider the application of the finite volume method (FVM) for such calculations [16, 17]. In this case, the computational area is divided by a grid, in the nodes of which unknown quantities are determined that characterize the parameters of the EF. The difference between FVM and conventional finite-difference methods lies in the fact that to obtain the solving system, the integration of the initial equations over the volumes of elementary cells, into which the computational area is divided, is used. One of the advantages of this approach is that the conditions at the media interfaces are fulfilled automatically, which simplifies the calculation of electromagnetic fields in inhomogeneous media.

Let us calculate the EF distribution in the vicinity of the lightning leader channel and lightning rods in a pre-thunderstorm situation. Since the leader channel moves relatively slowly towards the ground, such a calculation can be performed in a quasi-stationary approximation.

The equation to be solved is obtained by applying to the Maxwell equation

$$\operatorname{div} \vec{D} = \rho,$$

where $\vec{D}$—electrical induction, expressed through the strength of the EF $\vec{E}$ and electric potential φ:

$$\vec{D} = \varepsilon_0 \varepsilon \vec{E} = -\varepsilon_0 \varepsilon \, grad \, \varphi,$$

the operation of integration over V volumes of elementary cells into which the computational area is divided, and using the Gauss theorem. Let's finally write:

$$\int_S -\varepsilon \cdot \frac{\partial \phi}{\partial n} \mathrm{d}s = \frac{q_S}{\varepsilon_0}, \tag{2}$$

where S—surface enclosing the volume V; n—normal to the surface S; q_S—elementary charge placed on the surface S.

The system of equations obtained as a result of writing in the difference form equations of the form (2) for all nodes of the computational grid was solved by the iterative method of alternating directions using sweep.

To assess the accuracy of the numerical calculation, the following test system was used: an electrically conductive ellipsoid with a ratio of the major and minor semiaxes $a/b = 50$ and located in a homogeneous EF with a strength $E_0 = 1$ V/m and that its potential $U_0 = 1$ V. EF in such system can be described analytically by [18].

Since the rod has axial symmetry, a cylindrical coordinate system [19, 20] was used for the numerical calculation. Half of the original system was considered, such that its left boundary coincides with the axis of symmetry of the rod, the right boundary is located at a distance $R_{\max} = a$ from the axis, the upper boundary divides the major axis of the ellipsoid in half and coincides with its horizontal axis of symmetry, the lower boundary is removed from the upper one by a distance $Z_{\max} = 2a$. To take into account the ellipsoidal shape of the rod, the number of splits in the radial direction in the zone of the computational area $0 \le r \le b$ was chosen 10. It was assumed that the electrically conductive ellipsoid includes cells of the computational grid that lie completely inside its surface.

To reduce the dimensions of the computational domain when finding the EF distribution, the so-called uniaxially perfectly matched layer (PML) [21–23] are used on its right and lower boundaries. In such layers of thickness d, the permittivity is considered like a tensor that varies with the depth of the layers in accordance with the polynomial law, and its components in the directions of the coordinate axes Oz and Or are different.

So, for PML perpendicular to the Oz axis, in the range $z < 0$, the dependences of the z-th $\varepsilon_z^{PML}(z)$ and r-th $\varepsilon_r^{PML}(z)$ components of the tensor $\varepsilon(z)$ are written as [22, 23]:

$$\varepsilon_z^{PML}(z) = \varepsilon|_{z=0} \cdot k(z); \quad \varepsilon_r^{PML}(z) = \varepsilon|_{z=0} / k(z),$$

where $k(z) = 1 + (k_{\max} - 1) \cdot [|z|/d]^m$; m—index; $k_{\max}$—the maximum k value at the outer boundary of the PML; $\varepsilon|_{z=0}$—the ε value of the medium adjacent to the inner boundary of the PML.

Expressions for the tensor components in the PML perpendicular to the Or axis are written in a similar way. The values of the tensor components in the intersection zones of the PMLs are multiplied. According to the recommendations [21–23], 10 PMLs with parameters $m = 3$, $k_{\max} = 300 \cdot \varepsilon|_{z=0}$ were used in the calculations.

The limiting conditions are shown in Fig. 2. The calculated distributions of lines of equal potential when the rod is represented as an elongated ellipsoid are shown in Fig. 2a: the solid curves correspond to the numerical calculation, the dotted curves correspond to the analytical calculation. Comparison of the results of numerical and analytical calculations of the values of potentials and strength modules of the EF showed that the relative differences between the levels φ and $\vec{E}$ depend on the step size of the computational grid and at $\Delta = b$ (except for the step in the range $0 \le r \le b$, where $\Delta l = b/10$) do not exceed 4.6%. The difference between the numerical and analytical results is related to the stepwise approximation of the ellipsoid in the numerical solution. However, the discharge channels and lightning rods are closer in shape not to an ellipsoid, but to a cylinder. It can be seen that even at large ratios a/b, a decrease in several times the cross section of the ellipse at approaching its tops significantly affects the distribution of the EF. A comparison was made of the distributions of EF strengths in the above-described calculation system using these two representations in order to assess how much they differ from each other.

Figure 2b shows the numerical solution for the lines of uniform strength of the EF $\vec{E} = const$ in the same system as for Fig. 2a, but for a cylindrical rather than

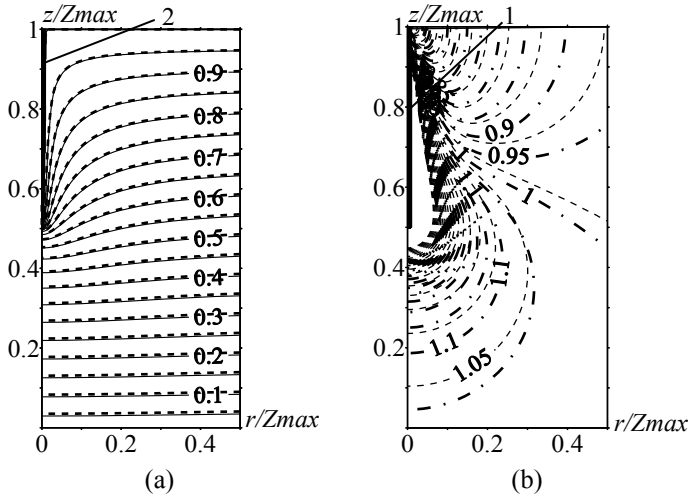

Fig. 2 Calculated distributions of lines of equal potential (**a**) and equal EF strength (**b**) at $H/R = 50$ (1—rod in the form of a cylinder, 2—rod in the form of an ellipsoid, — numerical solution for ellipsoid, – – – analytical solution for ellipsoid, –·–·– numerical solution for cylinder)

ellipsoidal rod shape. Dashed lines with dots correspond to the numerical solution for a cylindrical rod, and the dashed lines correspond to the analytical solution for an ellipsoid. It was believed that the radius of the cylinder $R = b$, and its height $H = a$. Calculations have shown that when the rod is represented as a cylinder, one step in space in the zone $0 \leq r \leq R$ is sufficient, equal to the radius of the cylinder $\Delta l = R$. For the considered parameters of the rods, when $H/R \geq 50$, the additional partition of the area $0 \leq r \leq R$ affects only the distribution of φ and $\vec{E}$ in a small area near the edge of the cylinder.

As can be seen from Fig. 2b, the distributions corresponding to the representation of the rod in the form of an ellipsoid and in the form of a cylinder differ significantly at $H/R \sim 50$.

For sufficiently long thin conducting rods, when the H/R ratio exceeds 10^2–10^3, the use of the usual representation of derivatives for finite difference methods in the form of differences in the values of the desired function at the nodes of the computational grid (piecewise linear approximation) leads to a complication of the problem. This is due to the fact that to provide an adequate description of the EF, the use of a computational grid is required, the step of which is of the same order as the radius of the rod, and for large values of H/R, the fulfillment of such condition is associated with a significant increase in the number of unknowns, as well as the number of iterations at their finding. To solve this problem, an approach similar to that described in [24] can be used, when it is considered that for a thin infinitely long rod, the change in the EF strength between the node of the computational grid located on its surface and the node adjacent to it in the radial direction does not occur along linear law, but inversely proportional to the distance of the nodes to the rod's axis. In [5], this approach was extended with respect to rods of finite length. The use of this approach makes it possible to calculate the EF with a significantly larger step of partitioning of the computational area, which is determined not by the radius of the rod, but by its length.

As an illustration, Fig. 3 shows the calculated distributions of lines of equal strength $\vec{E} = const$ in a system similar to that described above, but for the case when there is no PML at the lower boundary of the computational area ($z = 0$), and the potentials, which located on its nodes, equal to zero ("rod over a grounded plane" system) (Fig. 2b). Other system parameters and limit conditions are the same as described above.

Let's consider a cylindrical rod with a ratio of length to radius $H/R = 1000$. Such system simulates the presence of an electrically conductive discharge channel moving toward the ground. Solid curves in Fig. 3 correspond to the calculation performed taking into account the logarithmic decrease in potentials near the axis of the rod depending on the distance to it in the radial direction [5], the step of the computational grid is $\Delta = H/25$. The same figure shows the distributions $\vec{E} = const$, calculated using the usual for finite-difference methods representation of derivatives in the form of the difference of the desired functions at the nodes of the computational grid: dashed lines with dots obtained with the same step of the computational grid; dotted lines—with the step of the computational grid $\Delta = H/250$. As shown by the numerical experiments, a further decrease does not lead to a change in the potential

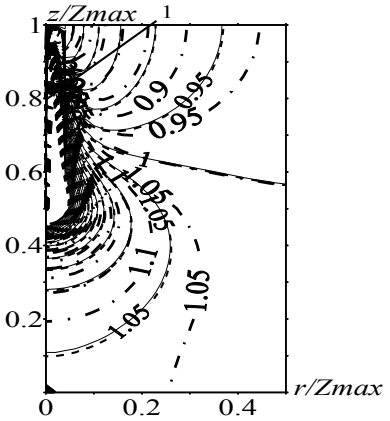

Fig. 3 Calculated distributions of lines of equal intensity of EF when the rod is represented as a cylinder ($H/R = 1000$) (— numerical solution according to the method [5] with a step in space $\Delta = H/25$; – – – numerical solution by the usual finite difference method at $\Delta = H/250$; –·–·– numerical solution by the usual finite difference method at $\Delta = H/25$)

values in the zone around the rod. In all calculations, the step along the coordinate in the direction of the Or axis in the area $0 \leq r \leq R$ was equal to $\Delta_1 = R$.

The numerical solution with a computational grid step having the same order as the rod radius can be considered basic in assessing the accuracy of the calculation using information about the logarithmic law of decreasing potential along the radius in the vicinity of the rod with a step Δ having the same order as the rod length.

As can be seen from a comparison of the solid and dotted curves, the distribution calculated using the usual finite-difference representation of derivatives with a sufficiently small step of computational grid practically coincides with the distribution obtained using a grid with step in 10 times larger, in the case of finite-difference representation of the equations takes into account information about the logarithmic nature of the decrease in the potentials of the EF in the zone, which is removed from the axis of the rod by one step of the computational grid. As can be seen from Fig. 3, the calculation at the same step of the computational grid ($\Delta = H/25$) using the usual finite difference method differs significantly from the basic solution of this problem.

As shown by numerical experiments [5, 23], at $H/R \geq 2 \cdot 10^4$ and $\Delta/R \geq 800$, the calculation results, when the rod is represented as a cylinder and using information about the nonlinear decrease in the potential in the direction perpendicular to its axis, coincide within 3% with the results analytical calculations of potentials in the vicinity of electrically conductive rods—ellipsoids. With such parameters, the step of the spatial grid, which depends on the length of the rod, is so much larger than its radius that the differences in the levels of potentials and intensities near the axis of the rod fall out of the scope of consideration. At the same time, as shown by numerical experiments, in the zone more distant from the axis, the distributions of EFs calculated when the rod is represented as an ellipse and a cylinder with the indicated H/R practically coincide. This means that if the zone directly adjacent to the surface of the rod is not interesting in the study, they can be modeled both with the help of a cylinder and with the help of an ellipsoid, with the considered ratios of the parameters of the electrically conductive rods.

2.2 EF Distribution in the Presence of Ionized Streamer Zone Near the Top of the Lightning Leader Channel

According to the sources [25, 26], the movement of the leader lightning with negative polarity forms by steps, and in the vicinity of the top of the leader there is an ionized (so-called streamer) zone, in which the space charge is concentrated. Numerical calculation methods make it possible to take into account the presence of such a zone, as well as to evaluate its effect on the increase in the EF strength in the vicinity of grounded objects when the lightning leader approaches the ground.

It is known that an increase in the EF strength at the top of the lightning leader channel can cause the development of a counter leader from ground objects [27]. To determine under what conditions this is possible, we calculate the distribution of the EF in systems simulating the movement of the leader lightning to the ground.

For the development of the leader channels, a minimum (let's call it E_{cr}) strength of the EF is required. According to the available data, the leaders of negative polarity develop at EF strength $E_{cr-} = 10^6$ V/m, and positive polarity—$E_{cr+} = 5 \cdot 10^5$ V/m [27].

As noted in [27], the development of numerous streamers from the top of the leader lightning, when it moves to the ground, leads to the fact that the streamer zone is filled with a space charge. It was also suggested there that the EF strength in this zone is close to homogeneous, since, as follows from the measurement results, the streamer velocity is about 10^5 m/s and practically does not change along the length of the streamer zone, and this is possible in a homogeneous EF, the strength of which is close to the minimum strength at which the development of streamer channels (E_{cr}) occurs.

Representing the streamer zone as an inhomogeneously charged sphere with a uniform EF, using the Gauss theorem, we can write the expression for the charge density in it in the form:

$$\rho(r) = 2\varepsilon_0 E_{cr}/r, \tag{3}$$

where r—distance to the top of the leader channel.

The streamer zone radius R_{str} is determined from the equation

$$U_L = \frac{1}{4\pi\varepsilon_0\varepsilon}\int_0^{R_{str}} \frac{4\pi r^2\rho(r)}{r}\mathrm{d}r = 2E_{cr}\cdot R_{str},$$

where U_L—potential of the top of the leader channel.

Then, for a negatively charged leader channel, R_{str} has the form:

$$R_{str} = 0.5 \cdot U_L/E_{cr}. \tag{4}$$

It is known that during a thunderstorm, the EF strength near the ground is about $E_0 = 2 \cdot 10^4$ V/m. We will consider lightning of negative polarity, the most typical for all latitudes, except for equatorial ones. The condition under which it is possible to develop an ascending leader of positive polarity from lightning rods is the achievement of the critical strength E_{cr+} in the movement zone of the lightning leader channel.

It is known that in local zones, adjacent to the tops of long thin conductive rods, the EF strength significantly (by 1–2 orders of magnitude) exceeds the applied voltage E_0. Therefore, the condition for reaching the strength at the top of the lightning rod, which is necessary to start the discharge ($E_{br} = 3 \cdot 10^6$ V/m), for lightning rods with $H/R \geq 300$–500 in thunderstorm conditions is certainly fulfilled. Then we can assume that the development of an ascending leader from a lightning rod with such parameters is possible if in the zone between its top and the head of the descending leader channel there is a continuous area (path for the streamer) in which the EF strength levels exceed E_{cr+}:

$$\left|\vec{E}_z\right| / E_{cr+} \geq 1, \tag{5}$$

where $\left|\vec{E}_z\right|$—EF intensity modules in the zone connecting the tops of the lightning rod and the lightning channel.

Consider an example of using the described EF calculations to assess the possibility of developing a counter leader from lightning rods. Radius of the leader lightning channel R_L is about several millimeters, and its length H_L has order of the average cloud height in thunderstorm conditions (H_L ~ 3–5 km). Since H_L/R_L exceeds 10^6, we will use the method for long leading rods described in [28] for calculation.

Let's consider a system with average parameters of lightning and lightning rods: $E_0 = 2 \cdot 104$ V/m, $H_L = 4000$ m, leader channel potential in the cloud area $U_0 = 80$ MV, leader channel top potential, taking into account the voltage decrease in it due to the presence of a gradient E_L in the channel: $U_L = U_0 - E_L \cdot H_L = 40$ MV, distance from the top of the leader channel to the top of the lightning rod $h = 40$ m, lightning height $H_R = 30$ m, charged streamer zone radius $R_{str} = 20$ m. For simplicity, we will assume that the leader channel is direct. The limiting conditions used in the calculation are shown in Fig. 4b, the dimensions of the computational area: $R_{\max} = 0.5 \cdot H$, $Z_{\max} = H$, computational grid step $\Delta = 1.25$ m. The results of calculating the lines of equal potential and equal strength of the EF in the vicinity of the top of the leader channel and the lightning rod are shown in Fig. 4.

To simplify the calculations, it was assumed that the radii of the leader channel and the lightning rod are the same: $R = 0.01$ m. As the numerical experiments have shown, for the described calculation system, in the presence of a charged streamer zone, variation of R in the range 0.01–0.1 m does not lead to a significant change in the values of φ and $\vec{E}$ in the vicinity of the top of the lightning rod.

The performed calculations showed that with the above-described parameters of the "leader—lightning rod" system, condition (5) is satisfied when the distance

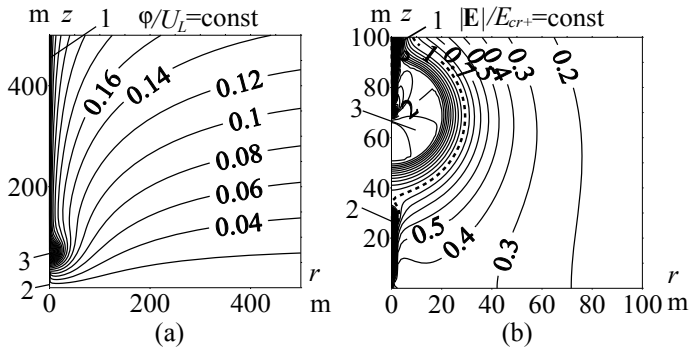

Fig. 4 Calculated distributions of lines of equal potential (**a**) and equal strength of EF (**b**) in the system simulating the approach of the lightning leader channel (1) to the lightning rod (2) in the presence of a charged streamer zone (3) ($H/R = 4 \cdot 10^5$, $R_{str} = 0.5 \cdot U_L/E_{cr} = 20$ m, $h = 2 \cdot R_{str+} = 40$ m, $E_0 = 2 \cdot 10^4$ V/m)

between the top of the lightning leader channel and the top of the lightning rod is less than

$$h \leq U_L/E_{cr-}. \tag{6}$$

In Fig. 4b, the thick dotted line shows the level $\left|\vec{E}\right|/E_{cr+} = 1$. As can be seen from this figure, $\left|\vec{E}\right|$ over the entire gap between the tops of the lightning rod and the lightning channel is greater than or equal to E_{cr+}. To determine, if condition (5) is always performed, numerical experiments were carried out for other values of the parameters of the lightning leader channel. Thus, the case of a relatively high EF intensity in a pre-thunderstorm situation was considered: $U_0 = 200$ MV, $U_L = 150$ MV, $R_{str} = 75$ m. EF calculations were also carried out at relatively low EF strength values: $U_0 = 60$ MV, $U_L = 30$ MV, $R_{str} = 15$ m. These calculations showed that the fulfillment of condition (5) is sufficient for the presence of an area between the tops of the leader channel and the lightning rod from $\left|\vec{E}\right|/E_{cr+} \geq 1$. Moreover, in this area, the EF levels do not change significantly during varying the height of the lightning rod H_R in the range 20–50 m.

3 Statistical Model of Electrophysical Processes During a Lightning Strike into Ground Objects

At present time the protection zones of lightning rods are determined in accordance with regulatory documents. However, the practical application of such standards for the choice of lightning protection means for extended objects is difficult. Damage

from a lightning strike to some facilities, such as launch complexes or storage tanks for petroleum products, can lead to significant material costs and even technological disasters [29–33]. Physical modeling of electromagnetic processes accompanying a lightning strike is quite expensive and, moreover, does not provide a complete representation of the phenomena occurring during a lightning strike. This necessitates the development of mathematical models of the processes accompanying the movement of the lightning leader channel and makes it possible to evaluate the reliability of the chosen lightning protection means.

One of the most common methods for assessing protected areas is the so-called electrogeometric method [34–36]. In this case, it is considered that the lightning rod zone lies inside the area, the outer boundary of which is formed by a "rolling sphere" with a radius $R_{last\ stroke} = 30$ m (last stroke is the average distance from which the "selection" of the strike place by lightning begins). Despite the clarity, this approach is a simplified representation of the lightning protection process, which does not take into account such important characteristics as, for example, the scattering of $R_{last\ stroke}$ values. At the same time, more complex models for predicting the processes of lightning movement to the ground [27], as a rule, are very far from solving the problems of practical lightning protection.

To simulate the statistical process of movement of the lightning leader channel in relation to the evaluation of the effectiveness of the developed lightning protection systems, the approach described in [37] can be used.

The model described in [37] is based on a generalization of experimental studies of pulsed high-voltage discharges in long gaps "rod-plane" and lightning [38–40]. At developing model, it was taken into account that the last stage of the movement of the lightning leader channel when it is oriented to a ground object (the so-called "last stroke" stage) begins when the streamed zone of the descending lightning leader channel reaches it. It is believed that the last hit is the process of moving the leader channel through the streamer zone. At the same time, it was taken into account that the magnitudes of the speed and acceleration of lightning depend on its potential, as well as on the angle between the velocity vectors of its movement and the EF strength in the surrounding space.

The model took into account that the corresponding grounded area can be struck by lightning in the considered numerical experiment if at least one of the two conditions described below is carried out. The first condition is to reduce the resistivity of one of the streamer channels to a level close to the resistivity of the lightning leader channel. The second condition assumes that one of the competing spark channels moving in the streamer zone of the lightning leader channel reaches the considered grounded area.

To describe the process of "selection" by the lightning leader of the strike place on the ground, a principle similar to the "Least Time—Maximum Probability" was used. It is believed that the probability of a lightning strike into a grounded area is inversely proportional to the time it takes the lightning leader channel to reach it at the final stage of its movement.

A rectangular computational grid (let's call it "grid 1") is overlapped on the area of the studied object. A rectangular computational grid (let's call it "grid 2") is also

overlapped on the area above the object, from where the development of leader lightning can occur. Moreover, the area of grid 2 significantly exceeds the area of the studied object, since it corresponds to the zone from which lightning can strike this object. When the model is running, the probabilities of a lightning strike into each cell of grid 1 from each cell of grid 2 are calculated. This takes into account the probability of occurrence of lightning carrying various potentials into the ground.

Comparison of the calculated and normalized ratios between the predicted number of lightning breakthroughs to the lightning rod and protected objects showed their coincidence within 10%.

Let's consider the use of this model to select a lightning protection system for a storage tank for petroleum products, which is a cylinder with a radius of 39 m and a height of 34 m. Using the developed model, several options for lightning protection systems for this object were considered.

At determining the probability of being struck by lightning, the N-predicted number of direct lightning strikes per year into an object with an area S_0 was used for a given geographical area:

$$N \approx N_m \cdot S_0, \tag{7}$$

where N_m—average number of lightning strikes per year per 1 km^2 in a given geographical area; S_0—object area.

Calculations were made for the case when annual average density of lightning strikes per square kilometer was equal to $N_m = 1$.

Figure 5 shows the calculated distribution of the predicted number of lightning strikes per year in a storage tank for petroleum products for the case of the absence of lightning protection facilities. At the same time, the total predicted number of lightning strikes on this object is such that lightning can hit it once every 6 years. The uneven distribution of the number of breakdowns along the outer tops of the tank is caused by the discreteness of the problem of nodes into which lightning strikes are calculated, and also due to the use of a rectangular computational grid relative to a cylindrical object.

Figures 6 and 7 show the calculated distributions of the predicted number of lightning strikes per year into the studied object in the presence of 1, 2 and 4 lightning rods, respectively, with 90 m height. In this case, the total predicted number of lightning strikes into this object is such that lightning can get into it once in 8, 11 and 19 years, respectively.

If, for safety reasons, it is still necessary to reduce the total predicted number of lightning strikes into the studied object, wire lightning rods can be used. The calculated distribution of the lightning strike probability in this case is shown in Fig. 7b (the height of the cables is 50 m). With such an arrangement of wire lightning rods, the predicted number of lightning breakthroughs to a given object is not higher than one per 100 years. Moreover, as shown by the computer simulation (Fig. 8), the use of 14 lightning rods with 90 m height, located in the same way as for the case shown in Fig. 7b, gives the predicted number of lightning breakthroughs to this object once every 43 years.

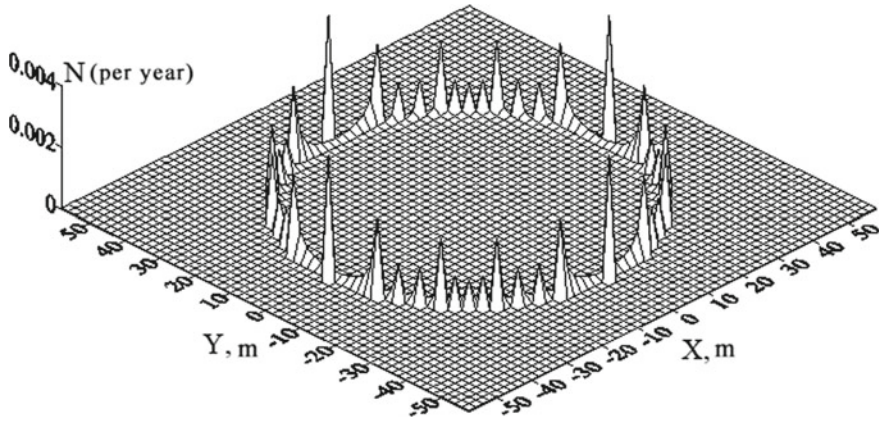

Fig. 5 Calculated distribution of the number of lightning strikes into the considered petroleum tank

The computer simulation of the processes accompanying the movement of the lightning leader channel at the last stage before the "selection" of the impact place of a grounded object made it possible to determine the predicted number of strikes of lightning rods and a non-standard protected object (tanks with oil products), to assess the degree of impact of the used lightning rods, and also to show that the use of wire lightning rods of the selected configuration makes it possible to practically eliminating lightning strikes into the studied object during the entire period of its operation.

As noted above, due to the complexity of the experimental study of the processes associated with the "choice" of the lightning leader channel of the strike place on the ground, a large number of mathematical models have been developed that describe these processes [41–43].

The most famous of them, quite simple and illustrative (the so-called electrogeometric method and the rolling sphere model) form the basis for the normalization of lightning rod zones, for example, in the USA [44]. These methods indirectly imply the presence of an ascending leader channel from ground objects.

However, targeted research related to the physical and mathematical modeling of ascending discharges from objects on the ground is not enough. As shown in a number of publications [4, 27, 45, 46], the discharge channels that develop from grounded objects in a thunderstorm situation play a significant role in orienting the lightning leader channel to ground objects. Thus, in France and Spain, there are regulatory documents that provide for testing the so-called active lightning rods, the principle of operation of which is supposedly based on the generation of counter leaders. However, the tests specified in these documents do not allow to fully take into account the electrophysical processes that accompany the emergence and movement of ascending leaders, and to evaluate the advantages and disadvantages of various lightning rods in a thunderstorm environment.

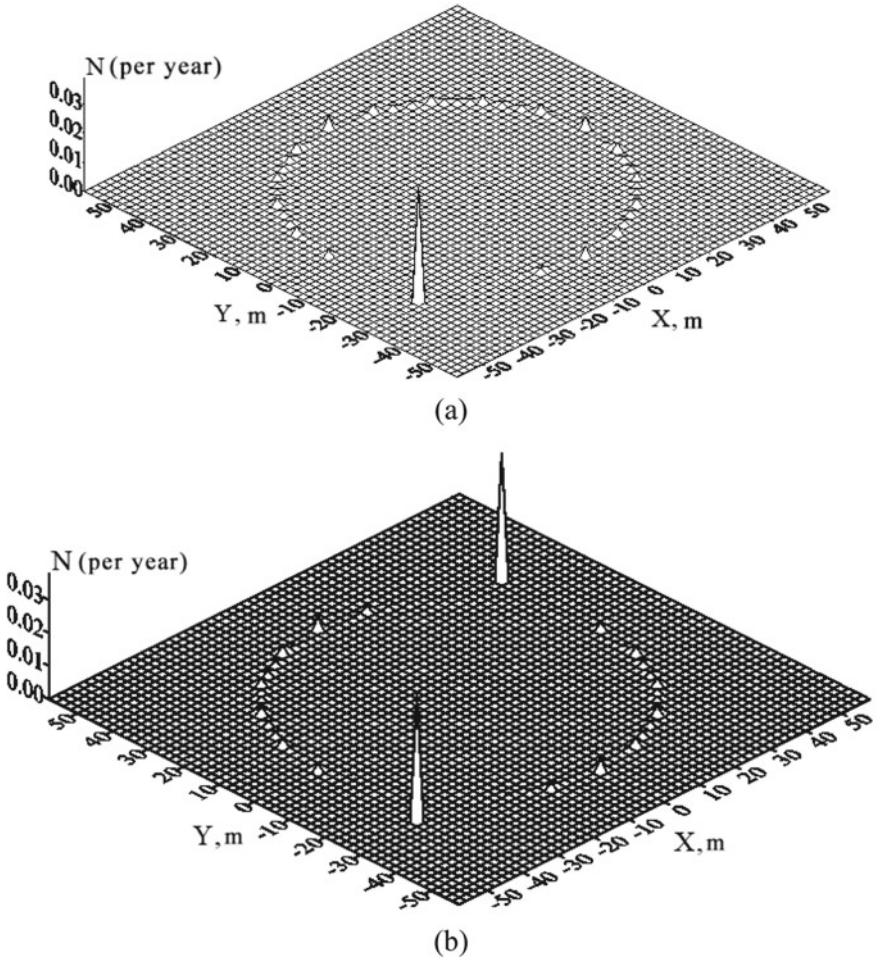

Fig. 6 Calculated distribution of the number of lightning strikes in the system: **a** tank—lightning rod with height 90 m; **b** tank—2 lightning rods with 90 m height

3.1 Statistical Modeling of the "Selection" of the Strike Place by Lightning

During statistically modeling the place of a lightning strike, it is necessary to carry out a number of mathematical experiments and vary all possible zones from which lightning leader channels can develop. In this case, one should take into account the distribution of lightning current values, determined by the levels of its potential, and the height at which its orientation to ground objects begins.

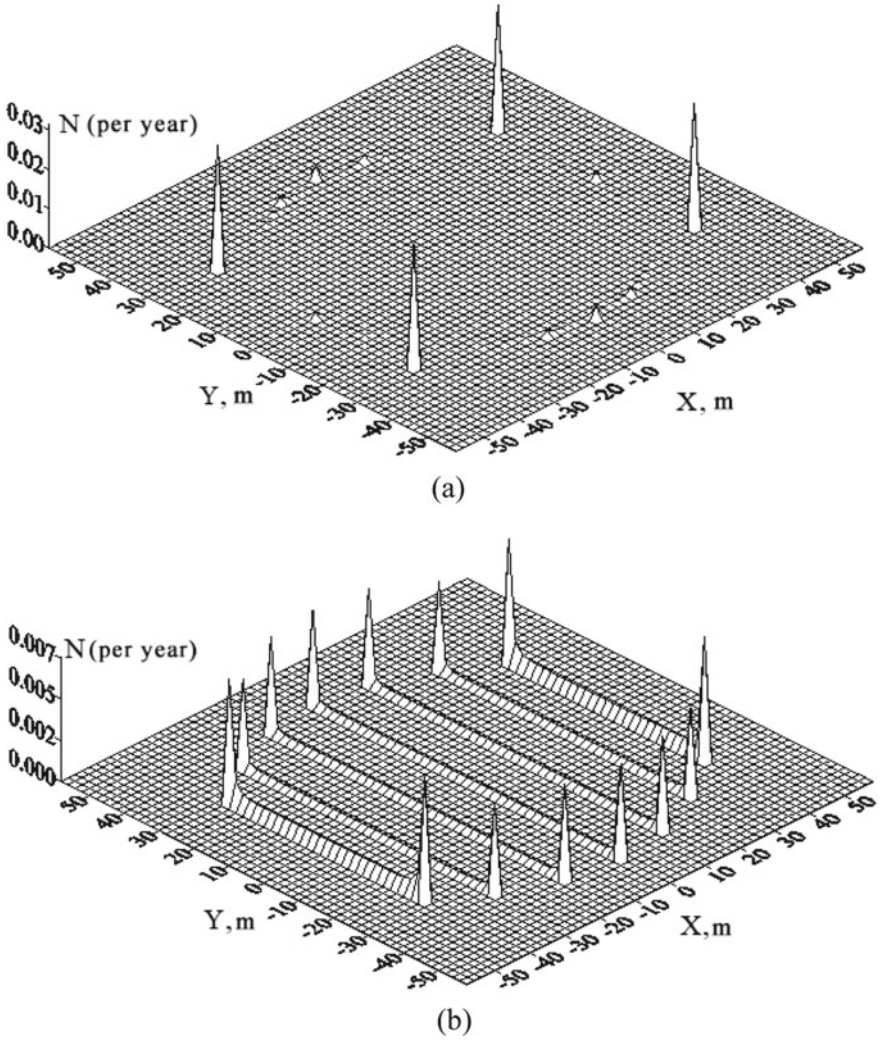

Fig. 7 Calculated distribution of the number of lightning strikes in the system: **a** tank—4 lightning rods with height 90 m; **b** tank—7 wire lightning rods

The value of the maximum reverse stroke current at the main stage of lightning I_m can be measured, and therefore there are systematic experimental data on the probability distribution of the lightning occurrence with a certain value of the discharge current [47–49].

In [50], it is indicated that the height of lightning orientation to ground objects (l_s) is determined based on the condition for reaching the "critical EF" E_{cr}, which is necessary for the breakdown of the gap. It is also noted there that E_{cr} must be greater than or equal to $0.5 \cdot 10^6$ V/m for negative leaders and $0.3 \cdot 10^6$ V/m for positive ones.

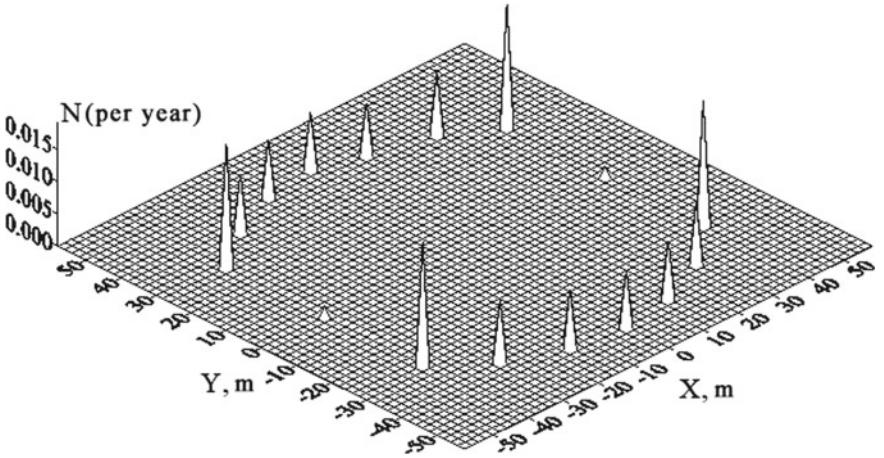

Fig. 8 Calculated distribution of the number of lightning strikes in the system "tank—14 lightning rods with height 90 m"

The value of E_{cr} is defined as being between the intensity of the EF required for the development of negative streamers E_{st-} and positive streamers E_{st+}. However, the EF intensity required for the development of a negative streamer is considered to be equal to E_{st-}.

The relationship between I_m and l_s is presented as:

$$l_S = a \cdot I_m^b, \tag{8}$$

where a, b—coefficients; l_s value measured in [m]; I_m value measured in [kA].

The values of the coefficients in Eq. (8) in different sources are considered equal: a—from 1.9 to 10, b—from 0.65 to 0.9.

At modeling the process of choosing the strike place by the lightning leader channel, its potential U_m is an important parameter. The U_m value is proportional to I_m, and there is a connection between I_m and U_m: $U_m \approx k_U \cdot I_m \cdot Z$ ($k_U \sim 1.7$, $Z \sim 500\ \Omega$). Then, assuming that $l_S = U_m/E_{st-}$, we get:

$$l_S \sim 0.8 \cdot I_m. \tag{9}$$

A similar approach for determining distances, from which the orientation of negative lightning leaders begins, describes as:

$$l_S = 1.9\, I_m^{0.9}, \tag{10}$$

although the intensity of the EF in the interval "leader—ground" is considered equal to E_{st+}.

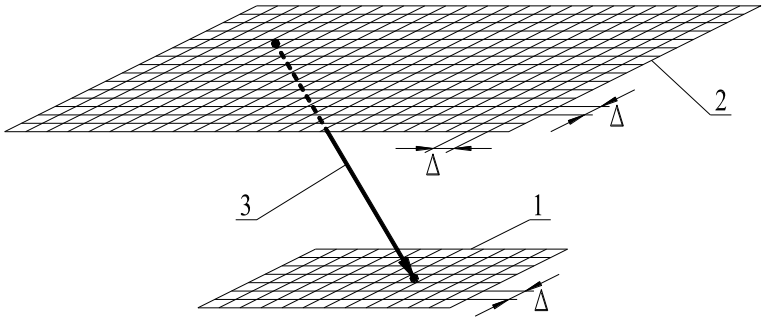

Fig. 9 Calculation system: 1—"area on the ground", 2— "thundercloud", 3—leader channel of lightning

For taking into account all possible options for a lightning strike into the study area ("area on the ground", Fig. 9), we divide its area (S_G) with a square grid with a step Δ. As a result, we get K_G cells with area $S_{Gk} = S_G/K_G = \Delta^2$.

We will assume that the probability of cell destruction is inversely proportional to the time of movement of the lightning leader channel to the corresponding node. Since lightning can strike the "area on the ground" from a larger area above it ("thundercloud", Fig. 9), to simulate all possible starting points for descending lightning leaders, we increase S_G by M cells, resulting in K_S cells and the corresponding them nodes ($K_S > K_G$). We assume that the probability of a lightning strike is the same within the k-th cell of the computational grid and is proportional to its area S_{Gk}.

In [51], based on the analysis of experimental data, it was shown that the root mean square (RMS) deviation of the breakdown voltage dispersion for discharge gaps 2–30 m long weakly depends on their length (6–7%). It is also noted there that the factors influencing the occurrence of the scattering can be variations in the moment of the emergence of the leader, the rate of its development, the length of the streamers, and the intensity in the leader and streamer zones. Based on these data, it is assumed that the relative dispersion of the discharge development times is $\varepsilon_S = 0.07$. We assume that a lightning discharge of a given potential U_i from the j-th node of the "thundercloud" can occur only in those nodes of the "area on the ground", the duration of the movement of the leader channel to which does not exceed more than $(1 + \varepsilon_S)$ times the minimum time of movement of competing discharge channels to all cells of the "area on the ground" in this numerical experiment: $t^i_{k,j} \le (1 + \varepsilon_S) \cdot t^i_{j_{\min}}$, where $t^i_j = \min\{t^i_{k,j}\}$. The defeat of all other cells in this numerical experiment will be considered impossible, and the probability of these events for these cells is considered equal to zero. Here, the nodes of the "area on the ground" into which a lightning breakthrough can occur have the k index; the total number of such nodes for a given numerical experiment which simulating a lightning strike with potential U_i from node j can be K^i_j.

Considering that in this numerical experiment there can be only one lightning strike, we will consider under $P^i_{k,j}$ probability density of a lightning breakthrough

into the k-th node of the "area on the ground" part of the lightning strikes into it from all possible cells "thundercloud" in this numerical experiment. We will proceed from the assumption that the value $P^i_{k,j}$ is inversely proportional to the propagation time to the k-th node on the ground of the lightning leader $P^i_{k,j} \sim 1/t^i_{k,j}$ and depends on the number and area of cells, the defeat probability of which in this numerical experiment is different from zero. For example, if the calculation indicated that the periods of movement of the leader lightning to each of the K^i_j nodes are the same, then the probability densities of the defeat of each of these nodes are the same.

Let us normalize the coefficient proportional to the probability of a lightning breakthrough into a node ($K\,P^i_{k,j}$) so that it is equal to 1 for the nodes, the movement time to which is minimal ($t^i_{j_{\min}}$), in this numerical experiment, and for nodes, the time of movement to which is more than $(1 + \varepsilon_S)$ times greater than $t^i_{j_{\min}}$ it was equal to zero:

$$K\,P^i_{k,j} = 1 - \frac{1/t^i_{j\,\min} - 1/t^i_{k,j}}{1/t^i_{j\,\min} - 1/[t^i_{j\,\min} \cdot (1 + \varepsilon_S)]} = 1 - \frac{1 + \varepsilon_S}{\varepsilon_S} \cdot \frac{1/t^i_{j\,\min} - 1/t^i_{k,j}}{1/t^i_{j\,\min}}. \tag{11}$$

In order to take into account the dependence of the probability of a lightning strike on the "area on the ground" node on the total number and area of cells that can be struck in this numerical experiment, we write $P^i_{k,j}$ as:

$$P^i_{k,j} = K\,P^i_{k,j} \cdot K_j. \tag{12}$$

The coefficient K_j is obtained from the condition of equality of the hitting probability one of the K_G nodes of the "area on the ground" in this numerical experiment:

$$\sum_{k=1}^{K_G} P^i_{k,j} = K_j \cdot \sum_{k=1}^{K_G} K\,P^i_{k,j} = 1.$$

Then

$$K_j = 1/\sum_{k=1}^{K_G} K\,P^i_{k,j}. \tag{13}$$

Let, for example, calculations show that when lightning moves from the j-th node of the "thundercloud", the duration of movement to two nodes of the "area on the ground" is significantly (by an order of magnitude or more) less than for all other nodes (for example, the coordinates of these nodes) correspond to the coordinates of the lightning rods), and,

$$t^i_{k1,\,j} = t^i_{j\,\min},$$

$$t^i_{k2,j} = (1/0.95) \cdot t^i_{k1,j} = 1.0526 \cdot t^i_{k1,j}.$$

Then from (11) we get: $K\,P^i_{k1,j} = 1$, $K\,P^i_{k2,j} = 0.236$. Substituting these values into (13), we get:

$$K_j = 1/\sum_{k=1}^{2} K\,P^i_{kjj} \approx 0.81$$

Let's finally calculate the probability of being struck by lightning for each lightning rod in this numerical experiment, substituting the obtained values into (12):

$$P^i_{k1,j} = K\,P^i_{k1,j} \cdot K_j \approx 0.81 \cdot P^i_{k2,j} \approx 0.19.$$

Thus, the total probability of this event is 1:

$$P^i_{k1,j} + P^i_{k2,j} = 0.81 + 0.19.$$

Knowing P_i the probability of occurrence of lightning with a current less than I_i, summing up all $P^i_{k,j}$ from lightning strikes with amplitudes I_i, whose leaders beginning from the j-th cells of the "thundercloud", we obtain an expression for the predicted number of lightning strikes in k-th node of the "area on the ground" in the form:

$$N_k = 10^{-6} \cdot N_m \cdot \sum_{i=1}^{M} \left\{ (P_{i+1} - P_i) \cdot \sum_{j=1}^{J} \left[\Delta^2 \cdot P^i_{k,j} \right] \right\}, \tag{14}$$

where M—number of intervals into which the range of lightning current variation is divided, and $\sum_{i=1}^{M} (P_{i+1} - P_i) = 1$; N_m—average annual number of lightning strikes per 1 km^2 of the earth's surface in a given geographical area; Δ^2—cell square, [m^2].

The time of movement of the descending leader channel from the j-th node of the "thundercloud" to the k-th node of the "area on the ground" is calculated as follows:

$$t^i_{k,j} = \left(L_{k,j} - l^i_S\right)/v^i_{0L\downarrow} + l^i_S/\left(v^i_{L\downarrow} + v^i_{L\uparrow}\right), \tag{15}$$

where $L_{k,j}$—distance between the k-th node of the "area on the ground" and the j-th node of the "thundercloud" at the beginning of the process of movement of the lightning leader channel from it; l^i_S—lightning orientation height with potential U_i, the leader channel of which moves from the j-th node of the "thundercloud"; $v^i_{0L\downarrow}$, $v^i_{L\downarrow}$—respectively, the speed of the descending leader channels of lightning with the potential U_i before and after the beginning of the through phase; $v^i_{S\uparrow}$—speed of the rising spark from ground objects for lightning with the potential U_i.

In the case when the conditions for the emergence and development of an ascending leader are not fulfilled, the value $v^i_{S\uparrow}$ in (14) is considered equal to zero.

3.2 Comparison of Experimental and Calculated Data on the Place of Discharge in Long Air Gaps

To compare the results of calculating the probabilistic places of damage by a high-voltage discharge in the presence and absence of a counter spark from grounded objects, let's consider the systems described in [27]. Despite the part these were carried out based on data obtained more than 70 years ago, they still have influence, if only because they form the basis of the regulatory document [52], which still regulates lightning rod zones. Almost all experiments, the results of which are given in [27], were carried out with a positive polarity voltage applied to a high-voltage electrode simulating the lightning leader channel. To substantiate this approach, [27] provides comparative data on breakdown points when a pulsed voltage of positive and negative polarity is applied to a high-voltage electrode for the same system parameters. In these experiments (the scheme is shown in Fig. 10a), a high-voltage rod electrode (1) was located above a grounded plane (2) at a distance $L = 1.6$ m from it and from grounded objects simulating a lightning rod (3), and protected object (4).

As follows from the experiments, when a voltage of positive polarity is applied to high-voltage electrode 1, approximately $N_2 = 0.80$ of all discharges hits the plane: $\sum N_2 \approx \approx 0.80$, for electrode 3—$N_3 \approx 0.08$ and for electrode 4—$N_4 \approx 0.12$ (where N_2, $\sum N_2$—particles of high-voltage discharges entering a separate cell on a grounded plane and all cells on a grounded plane, respectively; N_3, N_4—particles of high-voltage discharges entering the 3rd and 4th grounded electrodes. At determining $\sum N_2$, all probable breakdowns in all cells of the plane were summed up, therefore, despite the fact that N in Fig. 10a for individual cells of the plane is less than for rod lightning rods, the total share of predicted breakdowns in the plane is much larger ($\sum N_2 > \mathrm{N}_3$, $\sum N_2 > \mathrm{N}_4$). Mathematical modeling with using the method described above gave the following results: for the plane—$\sum N_2 = 0.76$, for electrode 3—$N_3 = 0.10$, for electrode 4—$N_4 = 0.14$ (Fig. 10a).

With this simulation, it was assumed that a counter spark from grounded objects would not develop, since the development of a spark of negative polarity requires an EF intensity that significantly (up to 2 times) exceeds the intensity in the streamer channel of the positive polarity descending leader.

It follows from the experiments that when a voltage of negative polarity is applied to the high-voltage electrode, when a counter spark can develop from object 3, approximately $N_3 \approx 0.85$ discharges strike electrode 3 and $\sum N_2 \approx 0.15$—the plane. Mathematical modeling using the technique described above gave the following results: for electrode 3—$N_3 = 0.84$, for the grounded plane (2)—$\sum N_2 = 0.16$ (Fig. 10b).

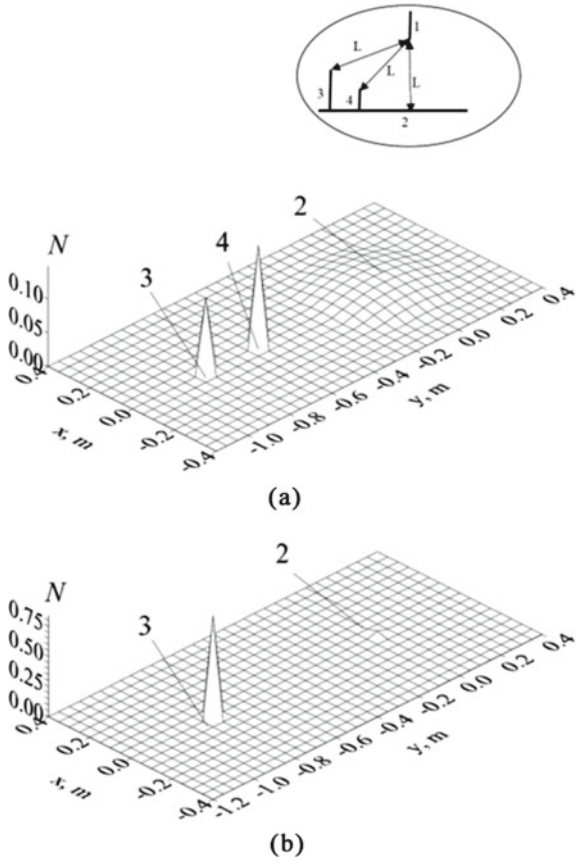

Fig. 10 Calculated distributions of the predicted distribution of the number of hits of downward discharges into objects (3, 4) located on the ground (2) when voltage is applied to the high-voltage electrode (1): **a** positive polarity; **b** negative polarity

During modeling, it was considered that a positive voltage $U = +0.7$ MV or a negative voltage $U = -1.4$ MV was applied to electrode 1. The speed of the streamers was set equal to 10^6 m/s, the capacitance per unit length of the leader in the through phase was 10 pF/m. The speed of positive descending leaders by the beginning of the through phase was considered equal to $v^i_{0L\downarrow} = 10^6$ m/s, the speed of negative descending leaders $v^i_{0L\downarrow} = 1.5 \cdot 10^5$ m/s, the speed of positive ascending leaders $v^i_{S\uparrow} = 0.3 \cdot 10^5$ m/s. In this case, the current in the through phase in the calculations was equal to 7 A when a voltage of positive polarity was applied, and 14 A when a voltage of negative polarity was applied.

Thus, the use of the described model made it possible to calculate the probability of a breakdown place when pulses of positive and negative polarity are applied to the gap "high-voltage rod—two rods on a grounded plane". Simulation and experiment data [27] coincide within 5–25%.

4 Study of Corona Processes at the Tops of Grounded Rods Simulating Protected Objects and Lightning Rods

The occurrence of corona discharges on the elements of electrical systems leads to a number of negative consequences. The most significant of these consequences is the loss of electricity. Another consequence is the appearance of high-frequency electromagnetic interference. High-frequency components of current, voltage and electromagnetic field, appearing through a corona discharge, have a negative impact on the operation of sensitive digital and electronic equipment, including automation and control systems. The most common corona processes are on the overhead power lines, so many works are devoted to this problem, for example, [22, 23, 53–55]. There are technical means to solve it, for example, [56–58]. At the same time, corona processes on sharp tops (systems of the "plane-point" type) are studied mainly with respect to an ozonizer [59–61]. Experimental studies of corona discharges were carried out mainly in systems with a "point-plane" geometry, with electrode-needles, to which EF of constant voltage of both polarities is applied. Usually, the EF intensity around electric power facilities is sufficient to create corona discharges around the most geometrically pointed elements of structures and equipment, for example, insulators, fittings, switches, high-voltage bushings, etc. The corona that develops around such elements may be caused by EF of direct current (DC) (positive or negative), such as resulting from a thunderstorm, or may be due to high alternating current (AC) voltage in the power system. The theory of corona processes is quite complex and has been repeatedly described in the literature, for example [62–66]. Thus, a corona discharge can be considered as consisting of two components:

- diffuse form of a gas discharge, which is often called a "luminous corona" (stationary component);
- incomplete plasma channels, which is often called "streamer corona" (impulse corona).

The first component can be easily measured with a microammeter, while the second component is measured with an oscilloscope and an impulse counter. Experimental studies of the dependence of the corona current on the applied EF and the geometry of the rod electrodes are described, for example, in [22, 64]. However, the conditions for corona initiation were not considered in these works.

5 Physical Modeling of Electromagnetic Processes During the Development of the Corona on Rod Electrodes with Different Vertices

5.1 Method for Measuring Corona Current

For physical modeling of the corona formation processes at the tops of grounded rod electrodes, a stand was used, the scheme and photographs of which are shown in Fig. 11. The experiments were carried out under conditions of normal temperature and atmospheric pressure (temperature $T = 20…23$ °C, atmospheric pressure $p =$ 1 atm).

This stand contains potential 1 and grounded surfaces 2 with dimensions 4 m × 4 m and located at a distance $d = 2.1$ m from each other, as well as a rod 3 installed on a grounded surface with height h and a vertex in the form of a sphere with radius R (Fig. 11). A high voltage U_0 was applied to potential surface 1, as a result of which an EF appeared in the zone between surfaces 1 and 2, which had an average intensity $E_0 \approx U_0/d$. To measure the corona current, a circuit was used that makes it possible to measure the number of pulses of the corona current in a time of 10 ms, equal to the duration of the half-cycle of the power frequency voltage.

A voltage proportional to the corona current flowing into the ground was taken from a low-inductance resistor $R_S = 75$ Ω. This voltage was applied with the help of measuring cable 4 to a high-frequency amplifier (HFA) 5 and a Rigol DS 1204B four-channel oscilloscope (Fig. 11b). At the opposite end, a low-inductance resistor $R_T = 25$ Ω was used to prevent reflection of pulses from the end of the cable. The equivalent input impedance of the measuring system was 37.5 Ω. The amplified signal triggered the generator of rectangular pulses 6. As a result, a sequence of rectangular pulses was formed, each of which corresponded to its own impulse of the corona current, and which was fed to the output of the pulse counter 9. Starting pulses of the beginning and end of the countdown of the counter were formed using a rectangular pulse generator 8 connected to 220 V (50 Hz) network through a phase shifter 7. Thus, by changing the phase of the mains voltage, the positions of the beginning and end of the pulse count were measured.

To ensure broadband registration of corona discharge pulses, the base of the ground electrode consisted of a short metal tube with a coaxial cable inside, as shown in Fig. 11b.

To provide a total resistance of 75 Ω, equal to the characteristic impedance of the cable, 6 low inductance resistors were connected in parallel at the top of the cable. The average corona current pulses were integrated and the resulting values were multiplied by the average pulse repetition frequency.

The DC component of the corona current was measured using an electromagnetic system microammeter (M266M) connected in series between the electrode rod and the grounded surface.

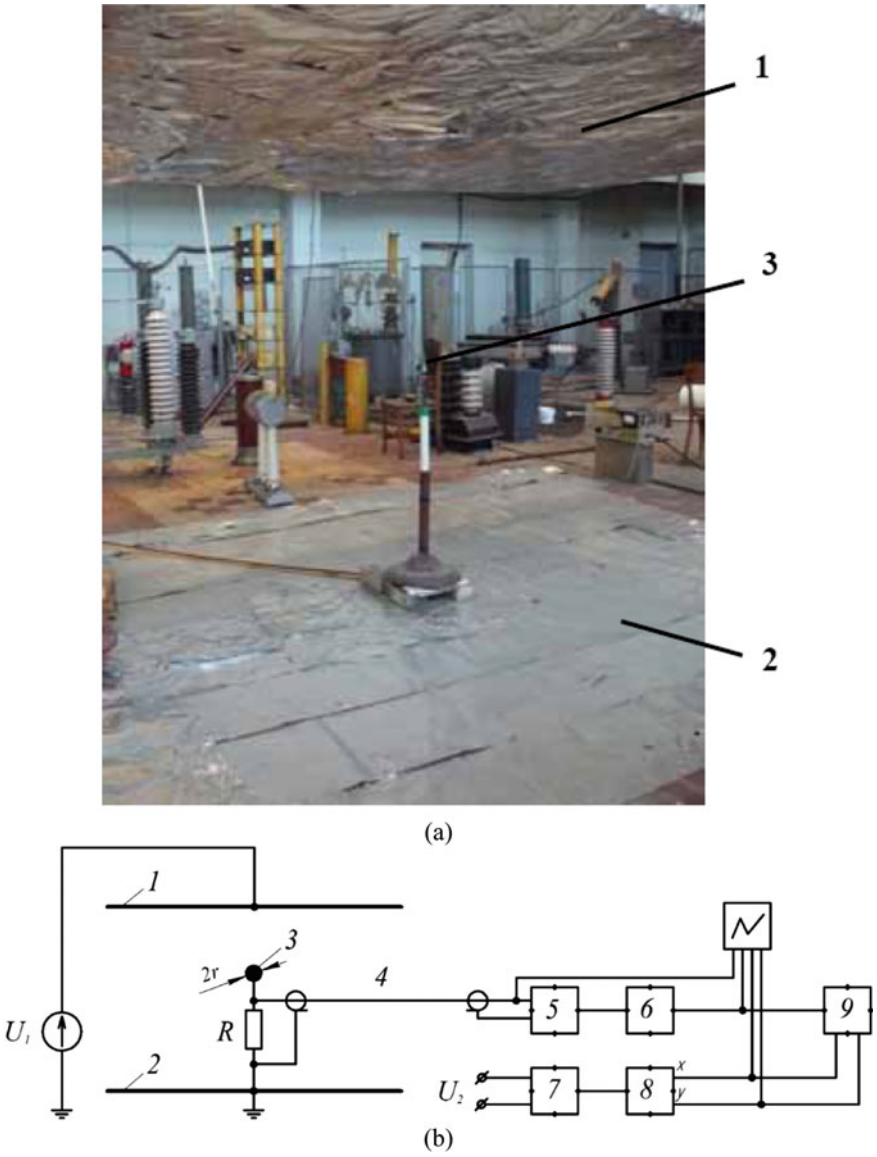

Fig. 11 Experimental stand for registration of corona current pulses: **a** appearance, **b** scheme of the stand (U_1—high voltage source (HV); 1, 2—potential and grounded electrodes-planes; 3—grounded rod electrode; R_S—shunt resistor ($R_S = 75\ \Omega$); 4—measuring cable; 5—high-frequency amplifier (U3-33); 6, 8—pulse generators (G5-54); 7—phase shifter; 9—frequency meter (F5034) in pulse counting mode)

5.2 Dependence of the Corona Current on the EF Nature

Corona current measurements were made for three cases, namely:

- I—a constant voltage of positive polarity was applied to the potential surface (maximum value—170 kV);
- II—a constant voltage of negative polarity was applied to the potential surface (the maximum value—170 kV);
- III—an alternating voltage of industrial frequency with an effective value of up to 100 kV was applied to the potential surface.

Figure 12 shows corona current oscillograms obtained from the ground electrode tip for three cases. The height of the grounded electrode *h* for all cases was equal to 1.2 m. The rod used in these tests had a conical top 0.14 m long, a base diameter of 0.04 m, and a radius of curvature at the end of the order of 0.1 mm.

For the first case (Fig. 12a), aperiodic corona current pulses were obtained, the average amplitude and duration at half height of which were practically independent of the applied voltage and amounted to about 2.27 mA and 28 ns, respectively.

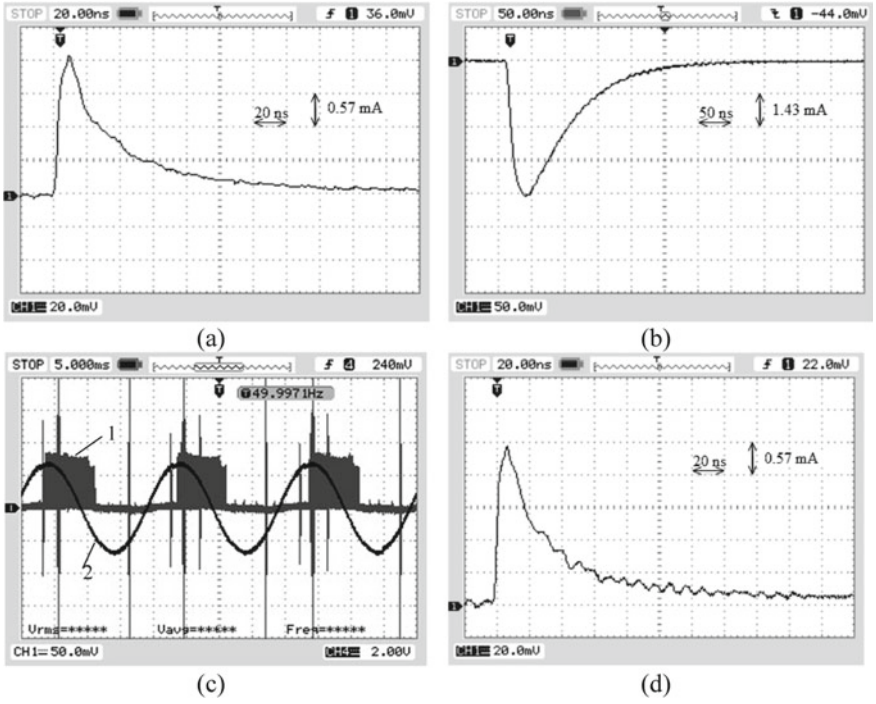

Fig. 12 Oscillograms of the corona current when a voltage of positive **a** and negative **b** polarity is applied to the potential surface, as well as an alternating voltage with frequency of 50 Hz **c**, **d** (on the oscillogram c: 1—corona current, 2—voltage applied between potential and grounded surfaces)

The average charge carried by the pulse was about 0.1 nC. The pulse transmission frequency increased in proportion to the applied voltage and, when a voltage of 50 kV was applied to the potential plane, was 3.18 kHz. The average corona current pulse was 0.3 mA. The constant component of the corona current, measured with a microammeter, was about 2.6 mA. Therefore, the corona current impulse was about 10% of the average DC current.

In case II (Fig. 12b), corona current pulses were observed only in a narrow range of applied voltages, i.e. from 30 to 40 kV. However, the average amplitude and duration at half height of these pulses were significantly higher than in case I (5.72 mA and 85 ns, respectively) On the other hand, the pulse repetition frequency was much lower—about 100 Hz. The average charge carried by the pulse was about 2 nC. The average pulsed corona current was approximately 0.2 mA, which is about 20% of the corona stationary current measured with a microammeter.

In case III (Fig. 12c, d), groups of corona current pulses appeared near the peaks of the positive half-cycle of the applied sinusoidal voltage, but they are almost absent at negative peak cycles. The positive half-cycle of the corona current pulse is very similar to that obtained in case I (application of a positive DC high voltage). When a high AC voltage of 50 kV RMS was applied to the potential area, the measured corona current was 2.85 mA with with a half-height duration of 30 ns It has been established that averaged charge, transported with pulse, was 0.1 nC. The pulse passing frequency at an RMS voltage level of 50 kV was significantly higher than in the previous two cases and was about 28.7 kHz. The average component of the corona current in this case was about 2.7 mA.

5.3 Dependence of the Corona Current on the Rod Geometry

The dependence of the corona current on the geometry of the rod was estimated using grounded rods with 6 different end radii R of rounding of spherical tops, namely: 0.0055, 0.00775, 0.009, and 0.0125 m, 0.01 at 4 values of their height h, namely: 1.2, 1.15, 1.05, and 0.93 m. A DC voltage U_0 of negative polarity up to 170 kV was applied to the potential surface, and the DC component of the corona current I_{cor} was measured. Table 1 presents the measurement results.

Figure 13 shows the dependence of the measured average value of the DC component of the corona current I_{cor} on the level of the applied DC voltage of negative polarity U_0 at the height of the grounded electrodes $h = 1.2$ m. Figure 14 shows the measured I_{cor} values at the same voltage as before, but with a fixed support radius $R = 0.009$ m and different rod heights. Measurements were also made for the case of the top of a grounded electrode with a height $h = 1.2$ m, made in the form of a cone with a height 0.14 m, a base diameter 0.04 m, and a top rounding radius of about 0.1 mm. However, all three voltage options (I, II and III) mentioned earlier were used for this configuration.

Figure 15 shows the measured dependences of I_{cor} on U_0—the module of the applied DC voltage of positive and negative polarity, for the case of a grounded

Table 1 Measured average values of the DC component of the corona current I_{cor} [mA] when a voltage of negative polarity is applied to the potential surface

U_0, kV	R, m	h, m			
		1.2	1.15	1.05	0.93
90	0.0055	2.5	2	–	–
100		4	4	2	–
110		8	7	4	2
120		13	11	7	4
130		20	17	12	8
140		30	26	18	14
150		42	38	27	20
160		61	54	40	30
170		85	74	56	42
110	0.00775	4	3	–	–
120		9	7	4	–
130		14	13	8	4
140		24	21	15	9
150		36	33	25	16
160		54	49	37	25
170		84	70	54	37
120	0.009	6	4	3	1.7
130		10	9	5	2
140		20	17	10	5
150		32.5	27	19	10
160		49	44	31	18
170		80	66	48	29
120	0.0125	2	1.3	–	–
130		5.5	3.5	–	–
140		13.5	11	5	–
150		24	20.5	13	5
160		36	33	22	12
170		55	50	36	21
140	0.015	8	4.5	–	–
150		19	14	6	–
160		33	27	15	7.5
170		53	40	30	16
150	0.019	5	–	–	–
160		21	13	2	–
170		43	33	15	0.3

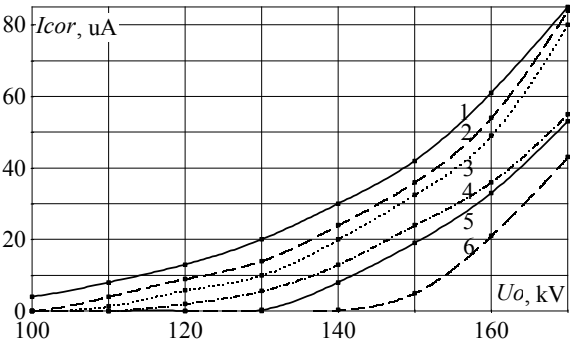

Fig. 13 Experimentally obtained dependences of the corona current (I_{cor}) on the modulus of the applied constant voltage of negative polarity (U_0) at different R radii of tops' curvature (electrode height $h = 1.2$ m): 1—0.0055 m; 2—0.00775 m; 3—0.009 m; 4—0.0125 m; 5—0.015 m; 6—0.019 m

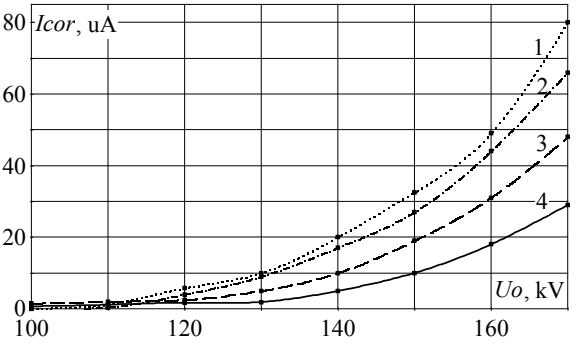

Fig. 14 Experimentally obtained dependences of the corona current (I_{cor}) on the module of the applied constant voltage of negative polarity (U_0) at different electrode heights (top rounding radius $R =$ 0.009 m): 1—1.2 m; 2—1.15 m; 3—1.05 m; 4—0.93 m

electrode with a height $h = 1.2$ m and a cone-shaped apex. Curve 1 corresponds to the case of applying a constant positive voltage to the potential plane, curve 2 corresponds to the negative polarity. As can be seen from Fig. 15, when a positive polarity EF is applied, the corona current is greater than when a negative polarity EF is used. However, the relative differences between the measured I_{cor} levels for these two cases do not exceed 20%.

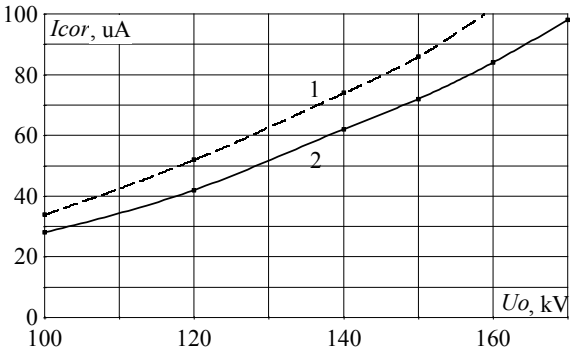

Fig. 15 Experimentally obtained dependences of I_{cor} on the level U_0—the module of the applied direct voltage of positive (curve 1) and negative (curve 2) polarity

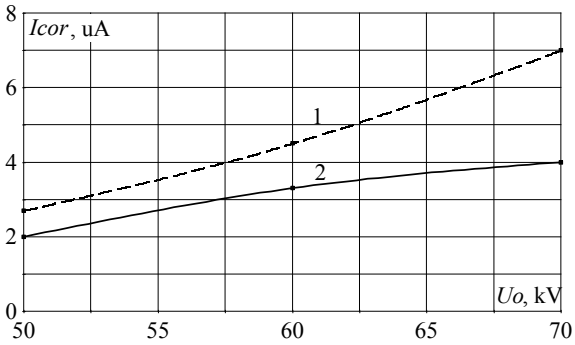

Fig. 16 The experimentally obtained dependences of I_{cor} on the level U_0—the applied DC voltage of positive polarity (curve 1) and the effective value of the power frequency AC voltage (curve 2) (the top of the grounded electrode has the shape of a cone with a height $h =$ 1.2 m)

Figure 16 shows the measured values of the corona current when a DC voltage of positive polarity (curve 1) and an AC voltage with a frequency of 50 Hz (curve 2) are applied. The measurements were made for the case of a grounded electrode of height h = 1.2 m with a cone-shaped apex.

As can be seen from Fig. 16, the levels of corona current, when an AC voltage is applied, is less than when a DC voltage of positive polarity is applied. Perhaps this is due to the fact that when the intensity levels of the applied EF are relatively small, corona occurs only on the positive half-waves of the sinusoidal voltage.

5.4 Experimental Results

From the experimental results, it can be concluded that corona processes on electrodes, consisting of a grounded rod located in an external EF, can be most typical for the case of a negative DC voltage of EF. This case represents the "average dependence" of I_{cor} on U_0 (or EF). The results obtained are average between those obtained with the application of a positive voltage and an alternating voltage with a frequency of 50 Hz.

6 Mathematical Modeling of Corona Discharges from Rod Electrodes

6.1 Comparison of Calculated and Experimental Results

In [67], the results of calculations of the strength of the EF at the tops of the rods with height h, curvature radius R, in relation to the strength of the applied average EF E_0 are given. The dependence $E_{\max}/E_0 = f(h/R)$ (where $E_{\max}$ is the maximum

strength at the top of the rod) is calculated, approximated by a polynomial. For the $h/R > 60$ range, the dependence can also be represented as a linear function:

$$K_{\max} = E_{\max}/E_0 \approx 0.6 \times h/R + 12.5. \tag{16}$$

To achieve conditions at the top of a grounded rod electrode under which breakdown develops in air under normal conditions in the zone of a weakly inhomogeneous EF [68], an applied EF with a strength $E_{ap} \geq 30$ kV/cm is required. Then from (16) it is possible to obtain a relation between the curvature radius R of the sharp top of a grounded object and its height h, upon fulfillment of which, for an object located in the zone of action of an EF of strength E_0 [V/m], suppression or a significant decrease in the corona intensity at a given object performed:

$$R/h > 0.6/\left(3 \cdot 10^6/E_0 - 12.5\right). \tag{17}$$

The last expression can be used to estimate the radius with which sharp tops should be rounded on objects of height h, which are located in the zone of action of the EF with strength E_0, so that corona discharges do not occur on them.

It can also be used to obtain an expression for the critical strength of the EF E_{cr}, which will lead to the appearance of a crown at the end of the rod electrode with a height h and a curvature radius R of the top, namely:

$$E_{cr}(h/R) \geq 3 \cdot 10^6/(0.6 \times h/R + 12.5). \tag{18}$$

Predictions for the appearance or absence of a corona on grounded rods of different heights with different tops rounding radii using formula (16) coincide with the results of physical modeling (Fig. 13). Thus, according to formula (16), the maximum excess of the EF strength on a rod electrode with a height of 1.2 m and a curvature radius of the top $R = 0.019$ m is about $K_{\max} = E_{\max}/E_0 \approx 50$. That is, corona discharges at the top of such an electrode should appear at an EF strength $E_0 \geq 30$ kV/cm/50 $= 0.6$ kV/cm. For the configuration considered earlier with $d = 2.1$ m, this EF corresponds to the applied minimum voltage. Comparison with experimental results under the assumption that the beginning of a corona occurs when the current exceeds $I_{\min} = 1$ mA (curve 6 in Fig. 13) shows that for this current level $U_0 = 150$ kV. This test voltage is slightly higher than $U_0^{\min}$, but they are not too different. All configurations for which the beginning of coronation was measured (Table 1) can be estimated in a similar way.

6.2 Dependence of the Corona Current on E_{max}

It is also important to evaluate the dependence of I_{cor} on $E_{\max}$, calculated in accordance with Eq. (16) for the corresponding values of h, R and E_0.

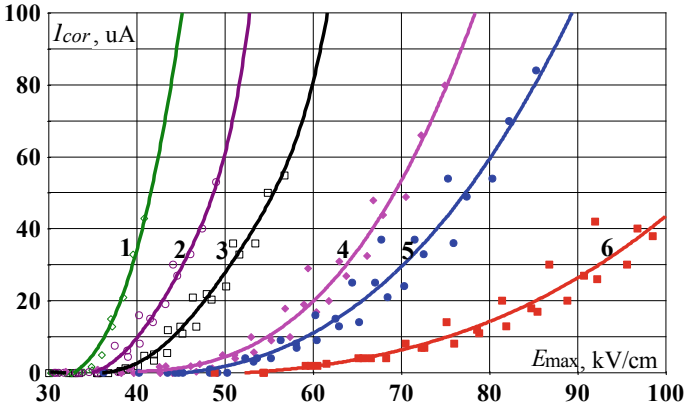

Fig. 17 Dependences of the corona current (I_{cor}) on the value of the maximum intensity at the tops of grounded rods (E_{max}) at different radii R of their curvature (1—0.019 m; 2—0.015 m; 3—0.0125 m; 4—0.009 m; 5—0.00775 m; 6—0.0055 m). Electrode height h and applied voltage levels U_0 varied. The dots show the measured values of I_{cor} at E_{max} calculated for the corresponding geometry and U_0, the curves show their approximation by polynomials

Figure 17 shows the dependences of the corona current on the level of the maximum intensity of the EF at the top of the grounded rod electrode, calculated in accordance with (16). The experimental data used in the construction of these dependences are given in Table 1. Each of curves 1–6 corresponds to electrodes with the same curvature radius R, 4 values of their height h (1.2 m, 1.015 m, 1.05 m, 0.93 m) and different levels of applied voltage of negative polarity U_0. With this U_0 variation, E_0 also changes, since d in all experiments was unchanged and equal to 2.1 m.

As can be seen from Fig. 17, the level of the EF maximum strength $E_{max} = K_{max}(h/R) \times E_0$ affects on the corona current value, and, therefore, the corona intensity. In this case, the lines corresponding to each curvature radius of the top of the grounded electrode have different curvature (see Fig. 1.2, curves 1–6). Based on the data shown in Fig. 17, it follows that the level of the EF maximum strength at the tops of the grounded electrodes cannot fully characterize the intensity of the corona processes, since this process, in addition to this parameter, is clearly affected by the value of the electrode curvature R. Moreover, the larger R, the lower levels of E_{max} achieve the same values of I_{cor}. Obviously, this is due to the fact that the volumes of the zones in which coronation occurs at the tops of the rods are proportional to R. In order to test this hypothesis, the calculations of the EF strength distributions in the considered systems were carried out.

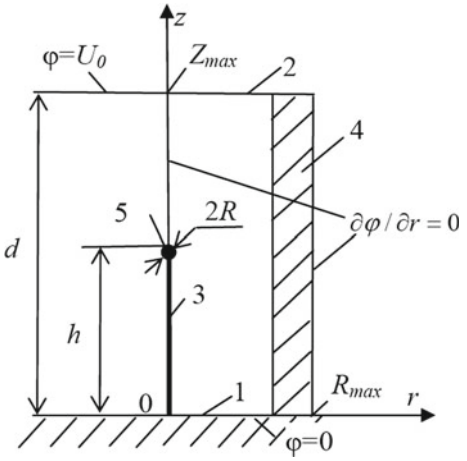

Fig. 18 Calculation system for mathematical modeling of the EF distribution on the tops of grounded rods (3) located in the system of potential (1) and grounded (2) planes, 4—PMLs, 5—electrode rounded top with radius R

6.3 *Dependence of the Initial Value of the Corona on the Volume of the Zone Due to the Critical EF*

To study the above effect, the EF spatial distribution in each of the considered configurations is calculated. Numerical calculations were performed using the system configuration with limiting conditions, as shown in Fig. 18. The use of axial symmetry of the system means that a cylindrical coordinate system can be used for calculations. Details of the calculation method are described in [69, 70]. Efficient calculations in the considered systems with different heights and curvature radii of the grounded electrode rods show that the spatial distribution can be represented as generalized variables, as shown in Fig. 19:

$$E^*\left(r^*, z^*\right) = E/E_{\max}, \tag{19}$$

where $r^* = r/R$; $z^* = [z - (h - R)]/R$; $E_{\max}$—maximum EF force at the end of the rod, calculated with the equation coefficient (16); and E—EF value at any point in space. As the comparison of the distributions $E^*(r^*, z^*)$, which made at different R and h, showed, they coincide in the vicinity of the tops of the grounded electrodes within 10–20%.

The volumes located within equal levels of the EF at $E^* = \text{const}$ (Fig. 19) were calculated using numerical integration. Dependency can be expressed as

$$V^*_{cor} = f\left(E^*\right), \tag{20}$$

where $V^*_{cor} = V_{cor}/V_0$; V_{cor}—volume of the zone in which the EF force exceeds a certain level E^*; and $V_0 = 4/3\pi R^3$—volume of the tip of the spherical rod.

Equation (20) can be replaced by a more convenient form by substituting $E^* = E/E_{\max}$ from Eq. (19) into Eq. (20):

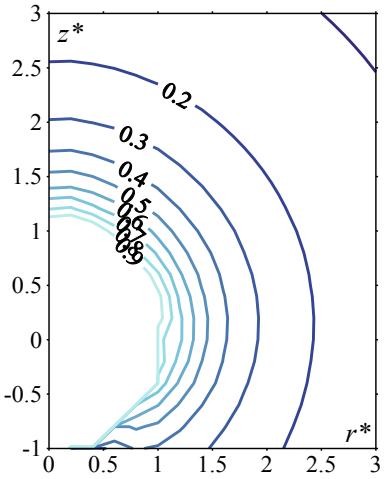

Fig. 19 Calculated distributions of lines of the same level of EF relative intensity E^* in coordinates $(r^*; z^*)$ at $R = 0.0125$ m and $h = 1.2$ m

$$V^*_{cor} = f(E_{\max}), \tag{21}$$

Equation (21) was used to obtain a volume in which the beginning of breakdown and corona discharges depends on $E_{\max}$. Figure 20 shows the dependence $V^*_{cor}(E_{\max})$, where $E_{\max}$ measured in [kV/cm]. This dependence can be approximated by a fourth-order polynomial for small values of $E_{\max}$ (dashed line in Fig. 20):

$$V^*_{cor}(E_{\max}) = -1.62 \cdot 10^{-7} \cdot E^4_{\max} + 4.07 \cdot 10^{-5} \cdot E^3_{\max} + 8.2 \cdot 10^{-4} \cdot E^2_{\max} - 0.19 \cdot E_{\max} + 4.31. \tag{22}$$

For large values of $E_{\max}$ ($E_{\max} > 150$ kV/cm), such a curve can be approximated by a second-order polynomial (solid line in Fig. 20):

$$V^*_{cor}(E_{\max}) = 0.0034 \times E^2_{\max} - 0.19 \times E_{\max} + 2.34. \tag{23}$$

Thus, the maximum EF strength at the end of the rod ($E_{\max}$) can be obtained by calculating $K_{\max}$ from condition (16) for a grounded rod with a given coefficient h/R and obtaining the multiplication of this value and the applied strength E_0, and then using Eq. (22) or (23) for obtaining V^*_{cor}.

Using this procedure, $V_{cor} = V^*_{cor} \times V_0$ was calculated.

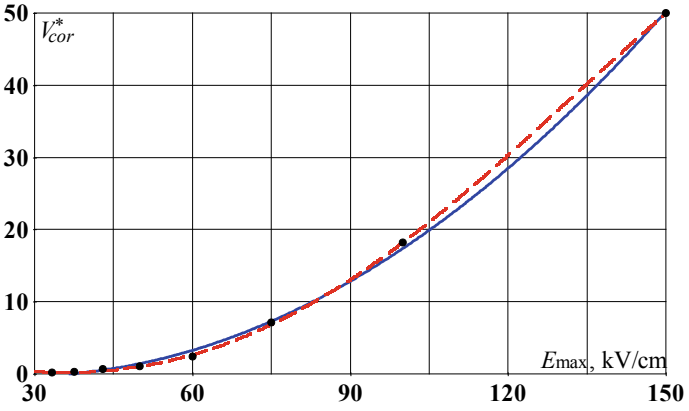

Fig. 20 Dependence of V^*_{cor} on the $E_{\max}$ value (points correspond to the calculated values, the solid line is the approximation by the 2nd order polynomial, the dotted line is the approximation by the 4th order polynomial)

References

1. Bonnell, J.W., Mozer, F.S., Delory, G.T., Hull, A.J., Ergun, R.E., Cully, C.M., Harvey, P.R.: The electric field instrument (EFI) for THEMIS. In: The THEMIS Mission, pp. 303–341. Springer, New York, NY (2009). https://doi.org/10.1007/978-0-387-89820-9_14
2. Lindqvist, P.A., Olsson, G., Torbert, R.B., King, B., Granoff, M., Rau, D., Tucker, S.: The spin-plane double probe electric field instrument for MMS. Space Sci. Rev. **199**(1), 137–165 (2016). https://doi.org/10.1007/s11214-014-0116-9
3. Ezawa, M.: A topological insulator and helical zero mode in silicene under an inhomogeneous electric field. New J. Phys. **14**(3), 033003 (2012)
4. Rezinkina, M.M.: Calculation of three-dimensional electric fields in systems with thin wires. Elektrichestvo **1**, 44–49 (2005). ISSN 00135380
5. Rezinkina, M.M.: Simulation of electric fields in the presence of rods with rounded upper ends. Tech. Phys. **60**(3), 337–343 (2015). https://doi.org/10.1134/S1063784215030238
6. Theberge, F., Daigle, J.F., Kieffer, J.C., Vidal, F., Chateauneuf, M.: Laser-guided energetic discharges over large air gaps by electric-field enhanced plasma filaments. Sci. Rep. **7**(1), 1–8 (2017). https://doi.org/10.1038/srep40063
7. Jiang, Z., Zeng, Z., Li, J., Liu, F., Li, W.: Simulation and analysis of GPR signal based on stochastic media model with an ellipsoidal autocorrelation function. J. Appl. Geophys. **99**, 91–97 (2013). https://doi.org/10.1016/j.jappgeo.2013.08.005
8. Rakov, V.A., Rachidi, F.: Overview of recent progress in lightning research and lightning protection. IEEE Trans. Electromagn. Compat. **51**(3), 428–442 (2009). https://doi.org/10.1109/TEMC.2009.2019267
9. Zeng, R., Zhuang, C., Zhou, X., Chen, S., Wang, Z., Yu, Z., He, J.: Survey of recent progress on lightning and lightning protection research. High Voltage **1**(1), 2–10 (2016). https://doi.org/10.1049/hve.2016.0004
10. Rezinkina, M.M., Knyazyev, V.V., Kravchenko, V.I.: Mathematical description of leader channel propagation for selection of model experiment parameters and lightning guard system. Tech. Phys. **52**(8), 1006–1010 (2007). https://doi.org/10.1134/S1063784207080075
11. Yu, A., Chabot, V., Zhang, J.: Electrochemical Supercapacitors for Energy Storage and Delivery: Fundamentals and Applications, p. 383. Taylor & Francis (2013)

12. Zhang, N., Yuan, P., ting An, T., Zhang, M., rong Chen, R.: The conductivity and propagation property of lightning leader tip. Atmos. Res. **245**, 105099 (2020). https://doi.org/10.1016/j.atmosres.2020.105099
13. Green, N.G., Jones, T.B.: Numerical determination of the effective moments of non-spherical particles. J. Phys. D Appl. Phys. **40**(1), 78 (2006)
14. Balanis, C.A.: Advanced Engineering Electromagnetics. Wiley (2012)
15. Rezinkina, M.M.: Growth of dendrite branches in polyethylene insulation under a high voltage versus the branch conductivity. Tech. Phys. **50**(6), 758–765 (2005). https://doi.org/10.1134/1.1947354
16. Wu, J., Traoré, P., Louste, C.: An efficient finite volume method for electric field–space charge coupled problems. J. Electrostat. **71**(3), 319–325 (2013). https://doi.org/10.1016/j.elstat.2012.12.004
17. Neimarlija, N., Demirdžić, I., Muzaferija, S.: Finite volume method for calculation of electrostatic fields in electrostatic precipitators. J. Electrostat. **67**(1), 37–47 (2009). https://doi.org/10.1016/j.elstat.2008.10.007
18. Masouri, Z., Hatamzadeh-Varmazyar, S.: Evaluation of current distribution induced on perfect electrically conducting scatterers. Int. J. Ind. Math. **5**(2), 167–173 (2013)
19. Babak, V.P., Babak, S.V., Eremenko, V.S., Kuts, Y.V., Myslovych, M.V., Scherbak, L.M., Zaporozhets, A.O.: Examples of using models and measures on the circle. In: Models and Measures in Measurements and Monitoring, pp. 127–156. Springer, Cham (2021). https://doi.org/10.1007/978-3-030-70783-5_5
20. Munir, A.: Computational approach for resonant frequency calculation of coaxial cavity resonator using cylindrical coordinate system-based FDTD method. In: 2015 International Conference on Quality in Research (QiR), pp. 73–76. IEEE. https://doi.org/10.1109/QiR.2015.7374898
21. Bérenger, J. P. (2007). Perfectly matched layer (PML) for computational electromagnetics. In: Synthesis Lectures on Computational Electromagnetics, vol. 2(1), pp. 1–117.https://doi.org/10.2200/S00030ED1V01Y200605CEM008
22. Rezinkina, M.M., Rezinkin, O.L.: Modeling of the electromagnetic wavefront sharpening in a nonlinear dielectric. Tech. Phys. **56**(3), 406–412 (2011). https://doi.org/10.1134/S1063784211030169
23. Rezinkina, M.M., Sokol, Y.I., Zaporozhets, A.O., Gryb, O.G., Karpaliuk, I.T., Shvets, S.V.: Mathematical modeling of the electromagnetic processes of the corona's formation during the operation of electric power facilities. In: Control of Overhead Power Lines with Unmanned Aerial Vehicles (UAVs), pp. 99–118. Springer, Cham (2021). https://doi.org/10.1007/978-3-030-69752-5_7
24. Taflove, A., Hagness, S.C., Piket-May, M.: Computational electromagnetics: the finite-difference time-domain method. In: The Electrical Engineering Handbook, vol. 3 (2005)
25. Gamerota, W.R., Idone, V.P., Uman, M.A., Ngin, T., Pilkey, J.T., Jordan, D.M.: Dart-stepped-leader step formation in triggered lightning. Geophys. Res. Lett. **41**(6), 2204–2211 (2014). https://doi.org/10.1002/2014GL059627
26. Sima, W., Li, Y., Rakov, V.A., Yang, Q., Yuan, T., Yang, M.: An analytical method for estimation of lightning performance of transmission lines based on a leader progression model. IEEE Trans. Electromagn. Compat. **56**(6), 1530–1539 (2014). https://doi.org/10.1109/TEMC.2014.2314772
27. Rezinkina, M.M., Knyazyev, V.V., Kravchenko, V.I.: Computation of the probability of lightning damage to ground objects. Tech. Phys. **52**(1), 59–64 (2007). https://doi.org/10.1134/S1063784207010100
28. Van Bladel, J.G.: Electromagnetic fields, vol. 19. Wiley (2007)
29. Kyrylenko, O.V., Blinov, I.V., Tankevych, S.E.: Smart Grid and organization of information exchange in electric power systems. Tekhnichna elektrodynamika **3**, 47–48 (2012)
30. Kyrylenko, O.V., Blinov, I.V., Parus, E.V., Trach, I.V.: Evaluation of efficiency of use of energy storadge system in electric networks. Tech. Electrodyn. **5**, 44–54 (2021). https://doi.org/10.15407/techned2021.04.044

31. Kyrylenko, O.V., Basok, B.I., Baseyev, Y., Blinov, I.V.: Power industry of Ukraine and realities of the global warming. Tech. Electrodyn. **3**, 52–61 (2020). https://doi.org/10.15407/techned2020.03.052
32. Baranov, G., Komisarenko, O., Zaitsev, I.O., Chernytska, I.: SMART technologies for transport tests networks, exploitation and repair tools. In: 2021 International Conference on Artificial Intelligence and Smart Systems (ICAIS), pp. 621–625. IEEE (2021, March). https://doi.org/10.1109/ICAIS50930.2021.9396055
33. Zaitsev, I., Levytskyi, A., Bogdan, K., Pavlo, R.: Optical fiber in nuclear power plants: applications to improve the reliability, safety and work stability of fault control instrumentation. In: Systems, Decision and Control in Energy III, pp. 123–138. Springer, Cham (2022). https://doi.org/10.1007/978-3-030-87675-3_7
34. Sreedhar, S., Srinivasan, V., Arulmozhivarman, P., Selvaraj, T.: Reliability assessment of lightning protection of renaissance architecture based heritage church in india using electrogeometric methods. In: 2021 Innovations in Power and Advanced Computing Technologies (i-PACT), pp. 1–7. IEEE (2021, November). https://doi.org/10.1109/i-PACT52855.2021.9696880
35. Martínez, J.M., Angarita, E.M.N., Alvarez, J.R.N., Crespo, M.H., Pertuz, P.J.F.: Lightning rod system: mathematical analysis using the rolling sphere method. Int. J. Power Electron. Drive Syst. (IJPEDS) **13**(1), 2829–2838 (2022)
36. Zhang, L., Wang, G., Zhang, W., Ma, Y., Guo, Z., Li, Q.: An electro-geometric model for lightning shielding of multiple wind turbines. Energies **10**(9), 1272 (2017). https://doi.org/10.3390/en10091272
37. Rezinkina, M.M.: Technique for predicting the number of lightning strokes to extended objects. Tech. Phys. **53**(5), 533–539 (2008). https://doi.org/10.1134/S1063784208050010
38. Meyer, H.K., Mauseth, F., Pedersen, A., Ekeberg, J.: Breakdown mechanisms of rod-plane air gaps with a dielectric barrier subject to lightning impulse stress. IEEE Trans. Dielectr. Electr. Insul. **25**(3), 1121–1127 (2018). https://doi.org/10.1109/TDEI.2018.007023
39. Aleksandrov, N.L., Bazelyan, E.M., D'Alessandro, F., Raizer, Y.P.: Dependence of lightning rod efficacy on its geometric dimensions—a computer simulation. J. Phys. D Appl. Phys. **38**(8), 1225 (2005)
40. Diaz, O., Hettiarachchi, P., Rahman, M., Cooray, V., Vayanganie, S.P.A.: Experimental study of leader tortuosity and velocity in long rod-plane air discharges. IEEE Trans. Dielectr. Electr. Insul. **23**(2), 806–812 (2016). https://doi.org/10.1109/TDEI.2015.005421
41. Vargas, M., Torres, H.: On the development of a lightning leader model for tortuous or branched channels–Part II: model results. J. Electrostat. **66**(9–10), 489–495 (2008). https://doi.org/10.1016/j.elstat.2008.04.011
42. He, J., Tu, Y., Zeng, R., Lee, J.B., Chang, S.H., Guan, Z.: Numeral analysis model for shielding failure of transmission line under lightning stroke. IEEE Trans. Power Deliv. **20**(2), 815–822 (2005). https://doi.org/10.1109/TPWRD.2004.839189
43. Cooray, V., Rakov, V., Theethayi, N.: The lightning striking distance—Revisited. J. Electrostat. **65**(5–6), 296–306 (2007). https://doi.org/10.1016/j.elstat.2006.09.008
44. National Fire Protection Association: Standard for the Installation Of Lightning Protection Systems. National Fire Protection Association (2011)
45. Bazelyan, E.M., Raizer, Y.P., Aleksandrov, N.L.: Corona initiated from grounded objects under thunderstorm conditions and its influence on lightning attachment. Plasma Sour. Sci. Technol. **17**(2), 024015 (2008)
46. Aleksandrov, N.L., Bazelyan, E.M., Raizer, Y.P.: The effect of a corona discharge on a lightning attachment. Plasma Phys. Rep. **31**(1), 75–91 (2005). https://doi.org/10.1134/1.1856709
47. Borghetti, A., Nucci, C.A., Paolone, M.: An improved procedure for the assessment of overhead line indirect lightning performance and its comparison with the IEEE Std. 1410 method. IEEE Trans. Power Deliv. **22**(1), 684–692 (2006). https://doi.org/10.1109/TPWRD.2006.881463
48. Martinez, J.A., Castro-Aranda, F.: Lightning performance analysis of overhead transmission lines using the EMTP. IEEE Trans. Power Deliv. **20**(3), 2200–2210 (2005). https://doi.org/10.1109/TPWRD.2005.848454

49. Mata, C.T., Bonilla, T.: Lightning risk assessment tool, implementation of the IEC 62305-2 standard on lightning protection. In: 2012 International Conference on Lightning Protection (ICLP), pp. 1–8. IEEE (2012, September). https://doi.org/10.1109/ICLP.2012.6344320
50. Uman, M.A.: The Art and Science of Lightning Protection. Cambridge Univ Pr. (2008)
51. Rakotonandrasana, J.H., Beroual, A., Fofana, I.: Modelling of the negative discharge in long air gaps under impulse voltages. J. Phys. D Appl. Phys. **41**(10), 105210 (2008)
52. IEC 62305-1: Protection against Lightning Part 1: General Principles (IEC 62305-1: 2010) (2011)
53. Rezinkina, M.M., Sokol, Y.I., Zaporozhets, A.O., Gryb, O.G., Karpaliuk, I.T., Shvets, S.V.: Physical modeling of discharges in long air gaps with the presence of the corona at the tops of grounded objects. In: Control of Overhead Power Lines with Unmanned Aerial Vehicles (UAVs), pp. 85–98. Springer, Cham (2021). https://doi.org/10.1007/978-3-030-69752-5_6
54. Zaitsev, I.O., Kuchanskyy, V.V.: Corona discharge problem in extra high voltage transmission line. In: Systems, Decision and Control in Energy II, pp. 3–30. Springer, Cham (2021). https://doi.org/10.1007/978-3-030-69189-9_1
55. Zhang, Z., Zeng, R., Yu, Z.: Measurement of corona characteristics and electromagnetic environment of ±800 kV HVDC transmission lines under high altitude condition. In: Progress in Electromagnetics Research Symposium: PIERS Proceedings, pp. 18–21 (2009, August)
56. Simmelvuo, M.K.: Electric power system suppressing corona discharge from viewpoint of environment, European Patent Office. International publication number: WO, 43708(12.05) (2005)
57. Rezinkina, M., Rezinkin, O., D'Alessandro, F., Danyliuk, A., Lisachuk, G., Sosina, E., Svetlichnaya, E.: Influence of corona on strike probability of grounded electrodes by high voltage discharges. J. Electrostat. **83**, 42–51 (2016). https://doi.org/10.1016/j.elstat.2016.07.005
58. Khaddour, B., Atten, P., Coulomb, J.L.: Numerical solution and experimental test for corona discharge between blade and plate. IEEE Trans. Magn. **43**(4), 1193–1196 (2007). https://doi.org/10.1109/TMAG.2006.890954
59. Chang, J.S., Lawless, P.A., Yamamoto, T.: Corona discharge processes. IEEE Trans. Plasma Sci. **19**(6), 1152–1166 (1991). https://doi.org/10.1109/27.125038
60. Tendero, C., Tixier, C., Tristant, P., Desmaison, J., Leprince, P.: Atmospheric pressure plasmas: a review. Spectrochim. Acta Part B **61**(1), 2–30 (2006). https://doi.org/10.1016/j.sab.2005.10.003
61. Patil, J.G., Vijayan, T.: Characteristics of high-tension-induced corona-discharge plasma in ozone generator diode. IEEE Trans. Plasma Sci. **38**(9), 2422–2427 (2010). https://doi.org/10.1109/TPS.2010.2057447
62. Bazelyan, E.M., Raizer, Y.P., Aleksandrov, N.L., D'Alessandro, F.: Corona processes and lightning attachment: the effect of wind during thunderstorms. Atmos. Res. **94**(3), 436–447 (2009). https://doi.org/10.1016/j.atmosres.2009.07.002
63. Sekimoto, K., Takayama, M.: Fundamental processes of corona discharge. J. Inst. Electrostat. Jpn **33**, 38–42 (2009)
64. Rezinkina, M.M.: Modeling of the dendrite shape variation with applied electric field strength in poly(ethylene). Tech. Phys. Lett. **26**(3), 196–198 (2000). https://doi.org/10.1134/1.1262789
65. Pinnangudi, B., Gorur, R.S., Kroese, A.J.: Quantification of corona discharges on nonceramic insulators. IEEE Trans. Dielectr. Electr. Insul. **12**(3), 513–523 (2005). https://doi.org/10.1109/TDEI.2005.1453456
66. Antao, D.S., Staack, D.A., Fridman, A., Farouk, B.: Atmospheric pressure dc corona discharges: operating regimes and potential applications. Plasma Sour. Sci. Technol. **18**(3), 035016 (2009)
67. Meng, X., Zhang, H., Zhu, J.J.: A general empirical formula of current–voltage characteristics for point-to-plane geometry corona discharges. J. Phys. D Appl. Phys. **41**(6), 065209 (2008)
68. Bazelyan, E.M., Raizer, Y.P.: Spark Discharge. Routledge (2017)
69. Tamm, I.E.: Fundamentals of the Theory of Electricity (1979)
70. Protection, L., Cooray, V.: The institution of engineering and technology. Published by The Institution of Engineering and Technology, London, United Kingdom